ISTITUTO NAZIONALE DI RICERCA METROLOGICA
Repository Istituzionale

Muography

Terms of use:

Publisher copyright

(Article begins on next page)

14 May 2024

MUOGRAPHY

Hiroyuki K. M. Tanaka[1, 2], Cristiano Bozza[1, 3], Alan Bross[1,4], Elena Cantoni[1,5], Osvaldo Catalano[1,6], Giancarlo Cerretto[1,5], Andrea Giammanco[1,7], Jon Gluyas[1,8], Ivan Gnesi[1, 9,10,11], Marko Holma[1,12,13,14], Tadahiro Kin[1,15], Ignacio Lázaro Roche [1,16], Giovanni Leone[1,17], Zhiyi Liu[1,18], Domenico Lo Presti[1,19], Jacques Marteau[1,20,21], Jun Matsushima[1,2], László Oláh[1,2], Natalia Polukhina[1,22], Surireddi S.V.S. Ramakrishna[1,23], Marco Sellone[1,5], Armando Hideki Shinohara[1, 24], Sara Steigerwald[1], Kenji Sumiya[1], Lee Thompson[1,25], Valeri Tioukov[1,26], Yusuke Yokota[1,2], Dezső Varga[1,27]

1. International Virtual Muography Institute, Tokyo, Japan
2. The University of Tokyo, Tokyo, Japan
3. Università degli Studi di Salerno, Salerno, Italy
4. Fermi National Accelerator Laboratory, Illinois, USA
5. Istituto Nazionale di Ricerca Metrologica, Turin, Italy
6. Istituto di Astrofisica Spaziale e Fisica Cosmica, Palermo, Italy
7. Université catholique de Louvain, Louvain-la-Neuve, Belgium
8. Durham University, Durham, UK
9. CREF, Centro Enrico Fermi, Roma, Italy
10. INFN LNF gruppo di Cosenza, Frascati, Italy
11. CERN, Geneva, Switzerland
12. Muon Solutions, Oulu, Finland
13. Kerttu Saalasti Institute, University of Oulu, Oulu, Finland
14. Arctic Planetary Science Institute (APSI), Oulu, Finland
15. Kyushu University, Fukuoka, Japan
16. Laboratoire Souterrain à Bas Bruit (LSBB), Rustrel, France
17. Universidad de Atacama, Copiapó, Chile
18. Lanzhou University, Lanzhou, China
19. Università di Catania, Catania, Italy
20. Institute of Physics of the 2 Infinities (IP2I), Lyon, France
21. MUODIM, Lyon, France
22. Lebedev Physical Institute, Moscow, Russia
23. Andhra University, Visakhapatnam, India
24. Federal University of Pernambuco, Recife, Brazil
25. The University of Sheffield, Sheffield, UK
26. National Institute for Nuclear Physics (INFN), Naples, Italy
27. Wigner Research Centre for Physics, Budapest, Hungary

ABSTRACT | Muography is a technique that takes advantage of the specific properties of a relativistic lepton called the cosmic-ray muon that is much heavier than the electron. Due mainly to their strong penetrating power and relativistic nature, cosmic-ray muons can be utilized for a wide range of technologies including imagery, positioning, navigation, timing (PNT), and secured communication in environments where most conventional techniques are unavailable. Cosmic-ray muons are universally present everywhere on the Earth and thus, muographic measurements can be conducted in the same manner globally and therefore have reproduced similar results regardless of the

countries where researchers conduct these measurements. This feature has enabled the muographic field to expand and grow, developing into a powerful tool to investigate natural phenomena, cultural heritage, and PNT worldwide. This Primer is intended as an introductory article to introduce new and established muographic techniques, case studies with some of the results obtained and some recent interdisciplinary advances. Data reproducibility and limitations are also discussed; additionally, there is a presentation of the outlook of developments in the future of muography.

INTRODUCTION

Muography, in its broadest definition, is an academic and applied field of research concerned with the use of naturally produced elementary particles, the cosmic-ray muons, which is applied to the research of natural objects and phenomenon as well as topics in human society, infrastructure, and culture. It includes the following muonic technologies (Figure 1):

(A) Muon-based imaging, mainly utilized in radiographic applications to visualize the internal structure of large objects by leveraging the strong penetrability of high-energy muons emitted by cosmic rays[1]. The terminology 'tomography' has sometimes been misused in various documents when applied to muon-based imaging. The word tomography etymologically consists of "cut or slice" (ancient Greek)[2] and "drawing". Unless the images acquired with muography are 3-dimensional images, the word "muon tomography" shouldn't be used. For example, the muographic images of volcanoes that can be seen in this reference[1] are not tomographic (cross-sectional) images but projected images. The usage of muon 'radiography' is also sometimes misleading since this word usually refers to x-ray imagery (Cambridge dictionary[3]). It is suggested that in the future researchers, when using the word "muon radiography", should clarify whether x-ray-like imagery with muons or imagery with muonic x-rays is meant. Vague descriptions or the wrong usage of terminology could potentially mislead researchers outside the muography community.

(B) Muometric positioning[4], navigation[5,6] and timing (PNT) that includes cosmic time synchronization (CTS)[7,8] and cosmic time calibration (CTC)[9],

(C) Wireless security with a secure authentication technique that implements a muogenic cryptographic protocol called cosmic coding and transfer (COSMOCAT)[10].

All muonic applications take advantage of the following seven properties, being essential characteristics of high-energy muons (which constitute the majority of the cosmic muon flux):

(1) strong penetration power (able to traverse up to a few kilometers of rock),

(2) path lines that travel practically straight regardless of the substance traversed,

(3) virtually constant flux regardless of the season or time of day,

(4) ubiquitous precipitation throughout the entire planetary surface,

(5) traveling at nearly the speed of light in vacuum,

(6) the true random number nature of the arrival time, and
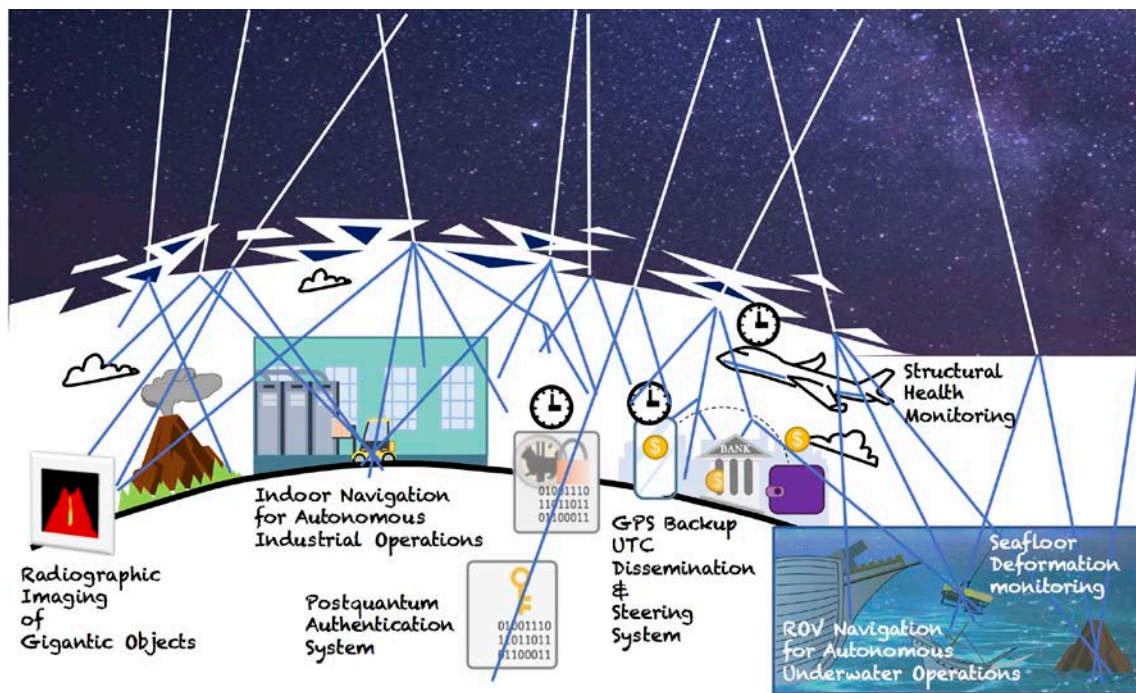
(7) multiple generation near the tropopause.

Fig. 1| Examples of the imaging, positioning, navigation and timing, and cryptographic technologies developed in the field of muography. The applications include imaging of geological, historical and industrial objects, indoor/underground/underwater positioning and navigation, universal time coordinated (UTC) dissemination and steering system, wireless sensor network, structural health monitoring, and tectonic seafloor deformation monitoring. ROV stands for a remotely operated vehicle.

After neutrinos, muons are the most numerous secondary particles at sea level[11]. However, unlike neutrinos, since muons are charged particles, they can be easily detected. A critical advantage of muography is that observations and measurements can be conducted without requiring an artificial source for the probes or signals since naturally occurring cosmic-ray muons are used. Most of these muons have high energies ($\geq$ multi-GeV) and their kinetic energies exceed their own mass. One of the consequences of this property is that, although muons at rest are short-lived (their intrinsic half-time is 2.2 μs), most cosmic muons live long enough to cross the entire atmosphere thanks to relativistic time dilation. In addition, since muons are 207 times heavier than electrons, they lose much less energy via radiative loss than the latter; thus, they can travel farther through matter than electrons if the incident kinetic energy is the same. Moreover, differently from other cosmic particles with similar mass such as the pions, they are insensitive to nuclear interactions. These features enable several applications including radiographic imaging of large

objects (ranging in size from nuclear waste barrels to volcanoes), muometric positioning, navigation and timing (PNT), and wireless security in indoor, outdoor, underground and underwater environments. This characteristic (the muon's strong penetration power) allows muons to investigate the content of shielding designed to prevent the passage of other forms of signals, and guarantees a high level of security against interference, jamming, and spoofing on global positioning system (GPS) signals. Under normal circumstances, it is impossible to generate artificial multi-GeV muons to raise significant noise in the data processing or to mimic true signals to interfere with muographic operations.

Besides its relatively inexpensive cost, the advantage of muography is a naturally abundant source in comparison to an artificially sourced particle/radio flux. Another advantage, for some applications, is the unpredictable nature of muon arrival times. In other words, the arrival time distribution of cosmic-ray muons is entirely random: one event occurs completely independently from the occurrence of another event[12]. In conjunction with its penetrative feature, cosmic-ray muons can be used as deliverers of encryption keys to confined and secure locations. This additional factor serves to increase the security level of cloud-based authentication[10].

This article is intended as an introduction to muographic imaging, muometric PNT, and muogenic encryption key distribution technique and the use of muons for applications in the Earth and planetary science topics as well as human, computer and social sciences. While the overview of these techniques is provided throughout this Primer, a reader in need of more specialized information is directed to refences[13,14,15] and references therein.

EXPERIMENT
This section provides an overview of the instrumental designs of muon imaging, PNT, and cryptography experiments. It also gives the reader some fundamental knowledge about muographic experimentation.

Muographic sources
As previously mentioned, cosmic-ray muons are (after neutrinos) the most abundant secondary particles at sea level. They are mainly generated as decay products of pions and kaons (which are in turn produced by nuclear collisions of the primary cosmic rays, protons and nuclei, with the nuclei of the atmosphere) in the following processes:

Charged pions $\quad\quad \pi^{\pm} \rightarrow \mu^{\pm} + \nu_{\mu}(\overline{\nu}_{\mu})$ $\quad\quad\quad$ ($\sim$100%), $\quad\quad$ (1)

Charged Kaons $\quad\quad K^{\pm} \rightarrow \mu^{\pm} + \nu_{\mu}(\overline{\nu}_{\mu})$ $\quad\quad\quad$ ($\sim$63.6%), $\quad\quad$ (2)

Neutral Kaons $\quad\quad K_{L} \rightarrow \pi^{\pm} + e^{\pm} + \nu_{e}(\overline{\nu}_{e})$ $\quad\quad$ ($\sim$40.6%), $\quad\quad$ (3)

$\quad\quad\quad\quad\quad\quad\quad K_{L} \rightarrow \pi^{\pm} + \mu^{\pm} + \nu_{\mu}(\overline{\nu}_{\mu})$ $\quad\quad$ ($\sim$27.0%), $\quad\quad$ (4)

Neutral Kaons $\quad\quad K_{S} \rightarrow \pi^{+} + \pi^{-}$ $\quad\quad\quad\quad\quad$ ($\sim$69.2%), $\quad\quad$ (5)

where the numbers indicated in parentheses indicate the branching ratio in the final state indicated. Most of the secondary particles are generated at an altitude of ~15 km. By

assuming a pion and kaon generation spectrum of $1.8 \times 10^4 E^{-2.7}$ (nucleons $m^{-2}s^{-1}sr^{-1}GeV^{-1}$)[11], the muon spectrum is approximated as follows[11]:

$dI/dEd\Omega$
$\approx 0.14 \, E^{-2.7} \, [1/(1+1.1 \, E \cos\theta/115 \text{ GeV})$
$+0.054/(1+1.1 \, E \cos\theta/850 \text{ GeV})] \, cm^{-2}s^{-1}sr^{-1}GeV^{-1}$ (6)

where the first and second terms indicate the contribution of pions and charged kaons, respectively. A muon at rest decays with a half-time of $\tau = 2.2$ µs. However, as predicted by Relativity, this decay constant extends as it accelerates to speeds on the verge of the speed of light in vacuum (c). Consequently, the muon's survival probability (W) and its decay lengths (L) are expressed by the muon's path length (L_{PATH}) as follows:

$W = \exp(-L_{PATH}/L)$,   (7)
$L = c\beta\gamma\tau = 3 \times 10^8 \text{ (ms}^{-1}) \times E/m \times 2.2 \times 10^{-6}$,   (8)

where E is the muon's kinetic energy and m is the muon mass. As can be seen in Eq. (8), only relativistic muons can arrive at sea level.

Muons lose their energies via the ionization and radiative processes (bremsstrahlung, direct pair production, and photonuclear reaction). Via the ionization process, the muon frequently collides with electrons losing a very small fraction of its energy in each collision. Fluctuations in the muon range are enhanced by the radiative processes, through which the muon loses a large random fraction of its energy. Critical energy is defined as the point where the ionization loss is equal to the bremsstrahlung loss. For example, the critical energy in air, H_2O, and SiO_2 are respectively 1.11 TeV, 1.03 TeV, and 708 GeV. Therefore, most cosmic-ray muons are subjected to the ionization process. For instance, vertical muons lose up to a few GeV of their energy in the atmosphere before they reach the surface of the Earth because the muon energy loss by air ionization is typically 2-3 $MeVg^{-1}cm^2$. The continuous slowing down approximation (CSDA) presented by Groom et al.[16] is convenient for calculating the analytical muon range:

$-dE/dX = a+bE$,   (9)

where the first and second terms indicate the contribution of the ionization and radiative processes, respectively. The parameters of a and b in Eq. (9) depend on the material muons travel through.

Muography simulations and data analysis
A typical Monte Carlo simulation chain starts from the generation of muons with realistic angular and momentum distributions. Approaches range from single-particle parametrizations to *ab initio* computations of the entire cosmic shower development in the atmosphere, as e.g. in the popular CORSIKA[17], CRY[18], and AIRES[19] programs.

The most crucial step in muography simulations is the passage of muons through dense material. GEANT4[19] is a framework that has been shown to be very accurate for simulating particle interactions through matter, in the energy range of relevance for

muography; however, it becomes too computationally expensive to use for very large volumes. For this reason, parametric simulations have been developed with the aim to reduce CPU time while preserving a fair level of accuracy (see e.g. reference[20]). For the purpose of muographic imaging, another interesting approach is "backward Monte Carlo", as implemented in PUMAS[21], where the simulation is run from the detector to the sky; that way, no time is wasted to simulate muons outside of the acceptance range. However, fake muons are not included in this strategy (which is not a problem if the muography setup filters them efficiently).

At the receiving end of the cosmic shower cascade, the geometry and the response of the detector also need to be simulated. While simple parametrizations of the detector efficiency may suffice in some cases, whenever a project is not statistics-limited, it becomes important to consider several experimental subtleties by performing a detailed simulation of the detector response. In the latter case, GEANT4[20] is the most commonly used tool.

Muography instrumentation
With the exception of detectors used for cosmic time synchronization (CTS), all muography detectors share a common feature: they are designed for tracking cosmic ray muons, and these components are specifically called 'trackers'. The azimuth angles (ϕ) and elevation angles (θ) of the incident particles can be computed by connecting a straight line between two vertex points ((x_1, y_1) and (x_2, y_2)) on planes in a space as follows:

$$\phi = \tan^{-1}[(x_1 - x_2)/z], \tag{10-1}$$

$$\theta = \tan^{-1}[(y_1 - y_2)/z], \tag{10-2}$$

where z is the distance of the planes. The positioning resolution of the vertex points is (Δx, Δy) and therefore gives the detector's angular resolution ($\Delta \theta$, $\Delta \phi$). If these vertex points are registered within a sufficiently narrow time window, it is identified as the same muon which has passed through the tracker.

Scintillation detectors, gaseous detectors and Cherenkov detectors are real-time detectors that have high timing resolution while nuclear emulsion detectors cannot be used for real time reading of muographic data; as such their usage is limited to imagery. The details of each detector type are discussed below. For sake of brevity, other detector technologies that are less frequently used in muography, such as semiconductor detectors, are not described in this Primer.

Scintillation detectors. With scintillation detectors, muon events are recorded as a flash of light generated by the incident charged particles that are then subsequently detected by photodetectors attached to the end of plastic scintillator strips[23,24,25,26] or scintillation fibers[27] configured in a grid to provide *X-Y* position-sensitive detectors (PSD) (Figure 2A). Muon trackers consist of two or more PSDs (Figure 2B). Particle trajectories can be

tracked by connecting two or more vertex points which are determined by the geometrical address of the scintillator strips and their corresponding muon arrival timings. The track reconstruction algorithm contains parameters related to the geometry of the detector (the positioning resolution, the size of the active area, and the distance between the scintillator bars). Photomultiplier tubes (PMT)[23,24], multi-anode PMTs[25], and silicon PMs (SiPMs)[26] have been used as photodetectors. Scintillation detectors yield timing data for individual muon events. Utilization of a radiation shield placed between PSDs can allow the system to reject the so called "electromagnetic component" of the cosmic-ray flux (i.e. electrons and photons) and to roughly determine the muon's momentum via Multiple-Coulomb Scattering (MCS)[23] (Figure 2C). This shielding configuration is used for other detector techniques. While rectangular scintillators (the cross-sectional shape is rectangular) (Figure 2A) are commonly used, a triangular scintillator extrusion (Figure 2D) is favored if more precise point resolution of the detector planes is required. WLS (wavelength shifting) fibers are embedded into each strip to transport the scintillation light produced by the passage of a charged particle to photodetectors (Figure 2D). When a muon passes through a counter, it will typically deposit charge in two adjacent triangular extrusions. By using a charge weighting algorithm (the relative amount of ionization deposited in the two strips), a point resolution (RMS) of better than 1 mm is obtained[28], thus the triangular scintillator implementation gives more than one order of magnitude better point resolution. Extruded plastic scintillator detectors, which were first used for geophysical studies[29], can be assembled into very large arrays (hundreds of m^2). Relatively large scintillator arrays had already been deployed in the volcano imaging project[30] in a fixed enclosure. This type of detector is used because of its cost effectiveness, ease of manufacture, robustness, and the flexibility to adapt to many different kinds of configurations. Since scintillation detectors have higher time resolution than gaseous detectors (another type of online muography detector), the muon's time of flight (TOF) can be precisely measured[4].
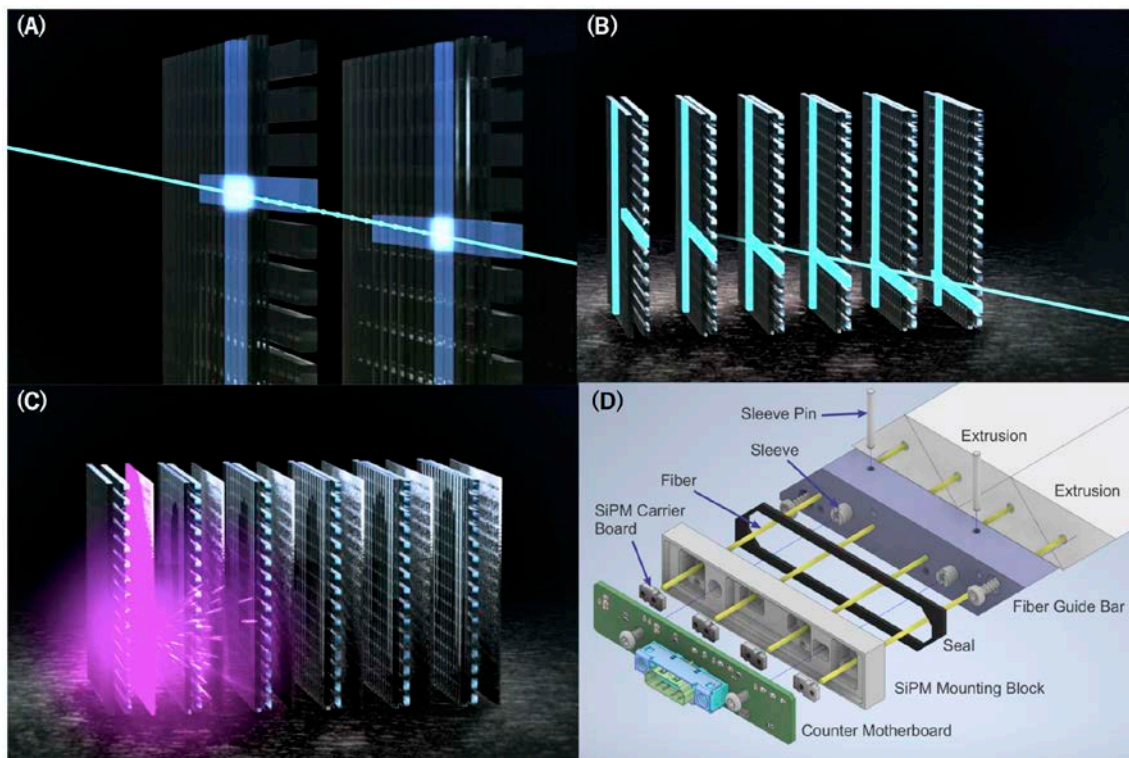
Fig. 2| (A) X-Y position from detector, **(B)** Muon tracker with multiple PSDs, **(C)** Illustration of rejection of electromagnetic components via Multiple-Coulomb Scattering, **(D)** Quad-counter| Diagram of Quad-counter showing the triangular scintillator extrusion, wavelength-shifting fiber readout and SiPM photon detector[28].

Gaseous detectors.

Gaseous detectors are a class of tracking systems which use gas as its active material, where free electrons, created by the traversing muon, are collected using electrodes, and multiplied in an avalanche process. These detectors have the main advantage of versatility, which earned the Nobel Prize for its inventor, Georges Charpak[31]. High energy and particle physics experiments are using such detectors extensively for over five decades[32]. The electron amplification from the detector active volume can take place either on thin anode wires[33], which is the basis of the Multi-Wire Proportional Chamber (MWPC), whereas it can also be amplified on micro-structures such as a thin mesh[34], or can create quenched sparks[35].

MWPC uses a 2-dimensional array of wires applied at high voltage. A conceptual view of gas amplification near wires is shown in Fig. 3A. The chamber is filled with a carefully chosen gas, such as an argon/methane mixture. MWPC-based muography systems have been developed at the Wigner Research Centre for Physics[36] and were successfully used in various applications[13] both on the Earth's surface and underground. Gaseous detectors are attractive options if time-dependent, high resolution measurement is required over a large surface. The main disadvantages are the complication of the tracking system (relative, for example, to emulsions), as well as the requirement of gas supply; hence gas bottles are usually attached to the system (Fig. 3B). This latter can be addressed through dedicated optimization [37], with a full tracking system consuming a fraction of the gas

volume that a human being would require. A contemporary gaseous muography system is indeed much more robust, mechanically and environmentally stable[38] than its laboratory-based predecessors.
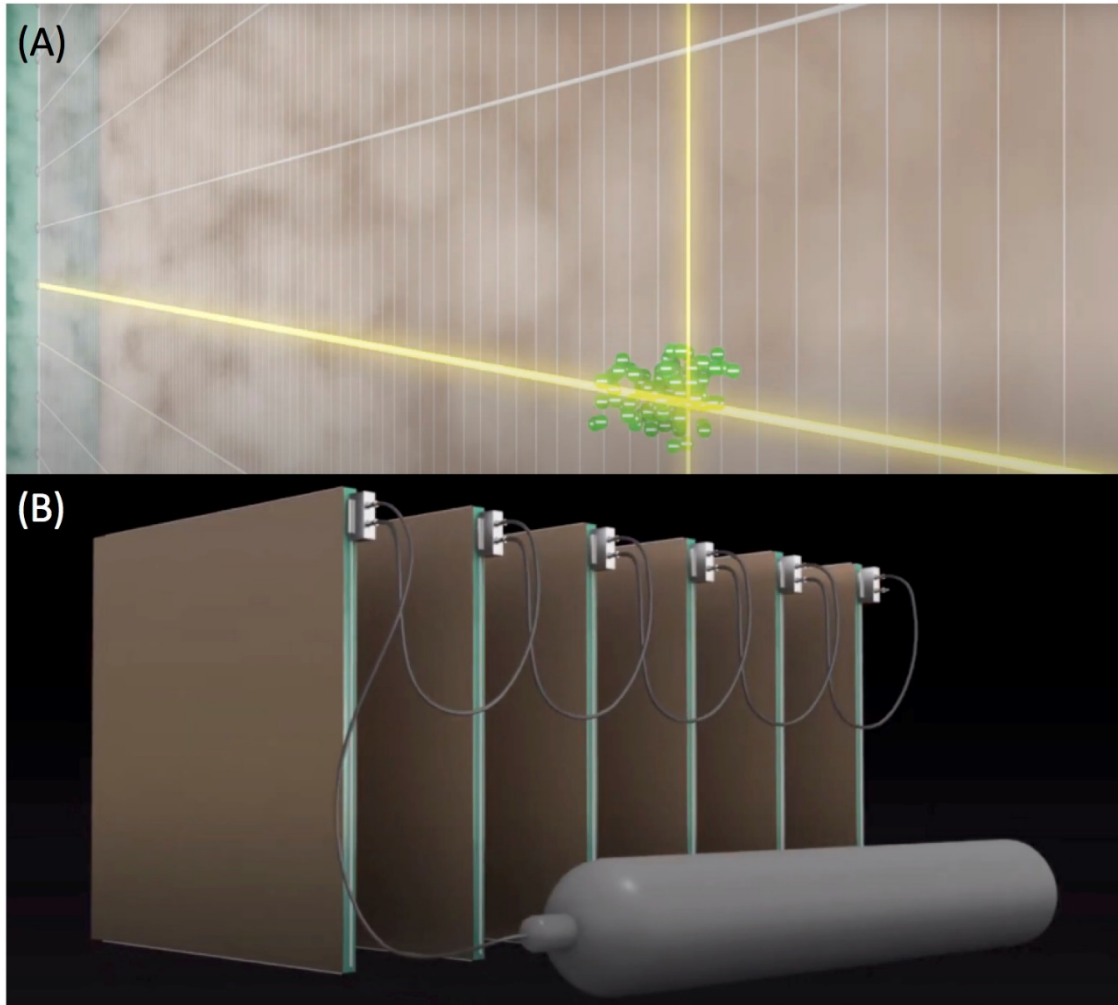

Fig. 3| Principle of the MWPC-based muography detector. Conceptual view of gas amplification near wires **(A)** and the system consists of MWPCs and a gas bottle are shown **(B)**.

The detector consists of a time projection chamber (TPC) with a diamond-like carbon (DLC) resistive Micromegas readout plane which presents interesting distinctive features, allowing the detector to have a wide angular acceptance with a light weight and reduced volume, making this design particularly well-suited for confined spaces or underground operation[39]. Currently, the Laboratoire Souterrain à Sas Bruit (LSBB) is deploying a network of muon trackers of this type. Once concluded, this will be one of the largest networks of muon trackers in the world applied to tomographic exploration of the critical zone up to 500 m deep.

Cherenkov detectors. A new and different approach to muon detector design is based on the detection of Cherenkov light emitted by relativistic cosmic ray muons in the

atmosphere. The example design has been developed by the Institute of Space Astrophysics and Cosmic Physics of the Italian National Institute of Astrophysics. Characteristic Cherenkov muon ring images are normally captured by IACTs (Imaging Atmospheric Cherenkov Telescopes)[40] (Figure 4). Muons, in fact, create typical annular patterns in the multi-pixel camera placed at the focus of the converging optics of a Cherenkov telescope. A given muon ring image, identified using simple pattern recognition algorithms, will contain all the information needed to reconstruct muon direction and energy.

All relativistic charged particles produce Cherenkov light as long as they travel faster than c/n, where c is the speed of light and n is the refraction index ($n \geq 1$). The muon energy is determined by the following formula:

$$E_\mu \text{ (GeV)} = 0.105 \cdot [(1-(\cos\vartheta^2)/n^2)]^{1/2}, \tag{11}$$

where ϑ is the emission angle[11]. Viewing can only be done in conditions of obscurity, but clouds do not adversely affect observations considering that the observations are made in the atmosphere in a region 80-100 meters from the telescope mirror. Therefore, even the presence of low density obstacles, including trees, (as long as they are farther than 100 m from the telescope) will not produce any attenuation of the collected light. A further advantage in using the muon ring Cherenkov method is that it results in an essentially background free observation due to the sharp ring produced by muons (Figure 4) while other cosmic particles have a more diffuse signature. If combined with the atmosphere data and target screening of the electromagnetic component data, these data ensure muons' detection and help avoid false positive count triggers If combined with the atmosphere data and target screening of the electromagnetic component data, these data ensure muons' detection and help avoid false positive count triggers. The limitation of this technique is that it requires a clear view between the target volume and the detector.
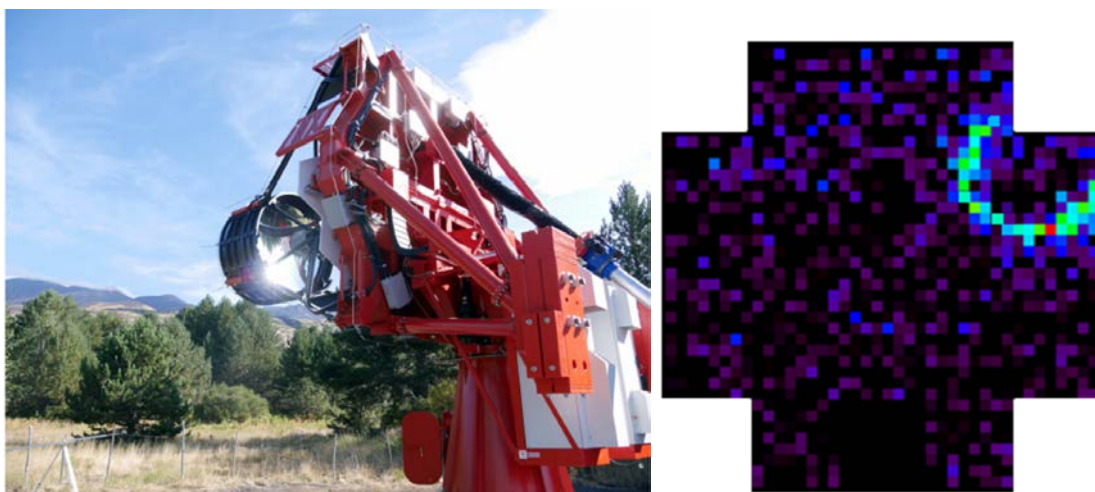

Fig. 4| Cherenkov detector| A mechanical structure that supports an optical system and a multi-pixel camera (left). A typical Cherenkov ring detected in the multi-pixel camera of the ASTRI-Horn telescope[41] (right). The radius of the ring corresponds to the

Cherenkov angle Θ. The position of the center gives the direction (position on the target) of the detected muon with respect to the telescope optics axis.

Nuclear emulsions. Nuclear emulsions[42] have a century-long history in particle physics, and have also been employed in many muographic imagery applications. The distinctive features of nuclear emulsions with respect to other, more common, particle detectors define rather clearly the scope of their applications for muographic imagery. Each ionising particle crossing a film (usually 50-100 μm thick) made of AgBr crystals interspersed in a gel leaves a trail of Ag+ ions. This latent image is made permanent by a chemical development process, which allows each ion to act as a site for the growth of metallic Ag in filaments. These filaments fold randomly, clustering in grains with a diameter of the order of 1 μm, appearing spheroidal when observed in transmitted light because of the diffractive resolution limit. The outcome is a 3D image of the full tracks of all ionising particles that passed through the film from its production until its development. The tracks are measured by a microscope with a tunable focal plane to reconstruct position and direction. For practical applications, nuclear emulsions are deposited on both sides of a relatively stiff transparent support (usually plastic or glass). With a 300-μm-thick plastic support base and two emulsion films, 50~100 μm-thick, coating both sides of the base, achieving directional precision in the order of 1 mrad is common, and the flatness of the support and its positioning precision dictate the real directional resolution of a nuclear emulsion muon detector. Figures 5A-5F show the basic concepts of a modular muon telescope based on nuclear emulsions. Angular acceptance in muography applications with this type of detector easily reaches cones of about 160° aperture with respect to the axis of the muon telescope. On the other hand, while time-tagging the tracks is theoretically possible, in practice it is quite difficult and in most applications just impossible, although several attempts have been made, e.g. by selectively accelerating the natural fading of the latent image or by moving supports that establish time consistency by varying alignments. As a consequence, nuclear emulsions are well fit to transmission muography applications, where a differential flux measurement has to be performed, and unsuitable for real-time muon measurements, as needed e.g. by volcano eruption alerts or by muon-scattering muography, which requires correlating in time the muon signals from two trackers.

In a single film there is no real way to discriminate among tracks collected during the exposure from all other tracks and grains accumulated in the emulsion from production until to development. Straight penetrating muon tracks crossing several nuclear emulsion films during the exposure are recognised by requiring tight alignment. Nuclear emulsions offer track position precision of the order of 1-3 μm, which is used to recognise matching patterns of tracks in different films of the stack and discriminate between straight muon tracks, random background and tracks from softer particles. Such high precision effectively compensates for the lack of track timestamping. The rejection power can be increased by inserting dense (Pb) spacers that act as absorbers and scatterers for soft particles. Using a stack of lead-emulsion layers the rejection power can reach 1 GeV with a still very slim (1-2 cm thick) detector thus reducing the soft particles background typical for muography data. Emulsion readout systems (Fig 5G) and data analysis frameworks for nuclear emulsions are already established and ready for use in many applications,
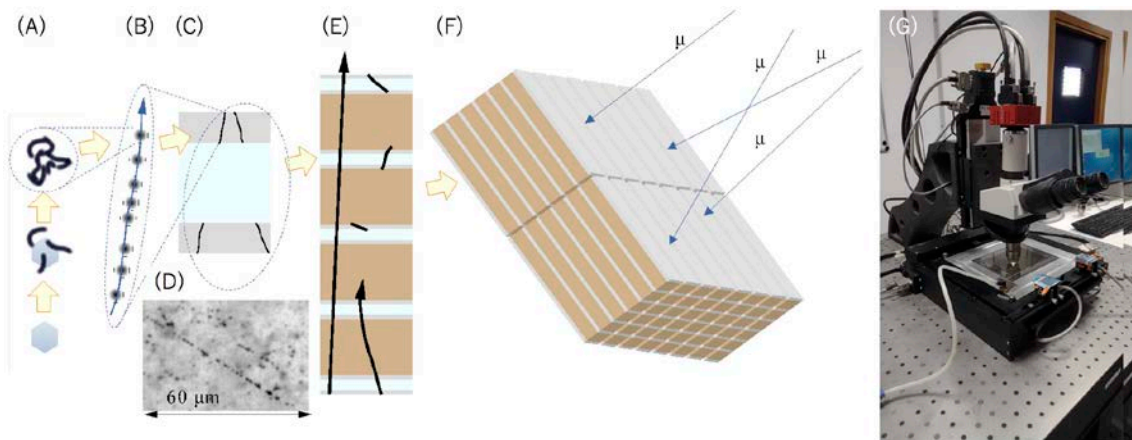
including muography.

Fig. 5| Concepts of muon detection by nuclear emulsion| (A) Growth of Ag filaments from the sensitised sites of an AgBr crystal touched by an ionising particle. (B) A trail of developed grains marking the track of an ionising particle in emulsion films. (C) An optical microscope image of a track. (D) Tracks on both sides of emulsion films coating a transparent support. (E) Ionising particle tracks in a stack of double-coated emulsion films interleaved with dense absorbers (iron, lead, tungsten): high energy muons travel with little scattering effects, whereas ambient radioactivity and soft (electromagnetic) particles are deflected or stopped in the absorber. (F) A modular muon detector is built by using several stacks and exposed to muons. (G) A modern emulsion readout system with a Cartesian (XY) robot moving stage on which emulsion films are held steady, while the Z axis is oscillating vertically to provide a fast optical tomography of a small view. By moving the stage, the whole area is scanned and a full readout of the collected data is provided. A dedicated workstation controls the motors and processes the images on the fly.

An advantage of nuclear emulsion detectors is their ability to work without electrical power and in the presence of electromagnetic disturbances. Exposing nuclear emulsion detectors in barely accessible sites, such as the flanks of volcanoes[43] and historical buildings[44] is relatively simple and requires little or no preliminary preparation of the site. On the other hand, nuclear emulsions are best operated above 5°C and below 30°C, since the emulsion melts at ~40°C. For environments with temperatures outside this range, other detectors have to be chosen.

Readout of nuclear emulsions is done by means of automatic microscopes, which are actually 3D cartesian robots with single or multiple cameras receiving the images of the emulsion film, held on a flat stage, provided by a suitable objective. Normally such images are taken with the microscope in motion, by utilizing stroboscopic illumination and/or electronic gating of the sensor sensitivity. The image sensors are capable of taking from 100 to 3,000 images per second, with varying resolution, usually in the range of 10^6 pixels. Readout speed has ramped up quickly in the past decades, from 0.1 cm^2/h (Track Selector/New Track Selector system[45,46] before the 1990's to 1 cm^2/h at the end of the century (Ultra Track Selector[47], System of Salerno), 20-72 cm^2/h around 2010 (European

Scanning System[48,49,50,51], Super-UTS[52]), 100 cm^2/h (Quick Scanning System[53], Large Angle Scanning System for OPERA[54]) near 2015 and 1 m^2/h (Hyper Track Selector[55] by the end of the past decade. The faster the readout system, the larger the area that can be analysed within reasonable timeframes; hence, the larger the muon detector, the larger the statistics available.

RESULTS

Muographic imagery

A certain number of muons stop in their pathway through a given object, depending on the object's size and density structure. The muons that pass through the object are captured behind the object by a muography detector. The generation of flat two dimensional images with this technique is called projectional muographic imagery. Since the range is a function of incident muon energy, it can be incorporated into the open-sky muon spectrum (Eq. (6)). Once both the muon path length and average density along the path are given, the areal density along the muon path (x) can be calculated by multiplying these values, and thus the minimum energy (E_c) of the muons which can penetrate through this areal density is determined with Eq. (9). Consequently, by integrating the open-sky spectrum I (E, θ, ϕ) from E_c to infinity we obtain the integrated muon intensity (Φ) recorded in each pixel of the muographic image, which represents the number of muons that have enough energy to escape from the target of interest such that:

$$\Phi = \int_{\phi}^{\phi+\Delta\phi} \int_{\theta}^{\theta+\Delta\theta} \int_{E_c}^{\infty} I(E, \theta, \phi) dE d\theta d\phi, \tag{12}$$

where θ, ϕ, $\Delta\theta$, and $\Delta\phi$, are respectively zenith angle, azimuth angle, zenith angular pixel size and the azimuth angular pixel size.

As can be seen in Eqs. (6) and (12), the flux available for muographic imagery is proportional to the size of the detector. Therefore, to perform muographic imagery of a large structure (such as volcanoes or the Great Pyramid of Giza) in an acceptable amount of time, large-scale muon detectors are required. This is due to the rate limitations of the cosmic-ray muon flux, the need to image over many different angles throughout the structure, and the need to accumulate enough data per effective voxel to minimize noise and maximize image fidelity. Generally, standard cargo containers[28,56] and prefabricated buildings[36] are used to house the large detector arrays since this is usually easy to implement and quite cost-effective.

On the other hand, aiming at smaller targets, several teams are focusing on developing portable particle trackers for muography. The eventual mass production and commercialization of muography detectors (particularly smaller and cheaper models) might open a large variety of currently unexplored or under-explored applications of both societal and academic relevance. Particularly advanced portable detector projects include MIMA[57], based on scintillating bars coupled with silicon photomultipliers, MUST2[58], a time-projection chamber based on micromegas, a project at Kyushu University[59] based on scintillating fibers, a project at Wigner Research Centre for Physics (RCP)[60] based on multi-wire gaseous detectors, and a Belgian project based on Resistive Plate Chambers[61].

There is a limitation to the resolution of muographic images. When a muon travels through matter, the Coulomb force between the muons and the nuclei in the medium leads to a large number of small deflections in the muon trajectories. As a result, their angular distribution broadens as they propagate through matter. However, due to the steep nature of the muon spectrum, the angular spread is suppressed to ~12 mrad (HWHM) after penetration of matter larger than 500 m.w.e. and this value is almost independent of the total areal density the muons have traversed[25]. Angular spread limits the positioning resolution at the target, e.g., 12 m at a distance of 1 km from the detector.

While radiography with x rays and γ rays is a standardized technique to inspect for a smaller-sized target volume, the cosmic-ray muon technique might offer a cheaper solution available under conditions where artificial radiation sources cannot be used. Such techniques have the potential, in the future, to be applied to investigating our daily-life objects by locating the cosmic muon's interaction within the target volume from scattering angles[62,63, 64] and secondary radiation emission[65].

Muometric PNT

Currently, PNT has been deeply disseminated to many social operations ranging from financial transactions to homeland security, but it thoroughly depends on GPS and other global navigation satellite systems (GNSS). However, since satellite-based positioning relies on low-power and unencrypted signals, these are susceptible to both intentional and unintentional disruption. Therefore, an alternative PNT system is in demand as a GPS backup to increase the resiliency of critical infrastructure by helping to reduce GPS vulnerabilities in the future[66].

Positioning and navigation. Most cosmic ray muons have a velocity close to the speed of light in vacuum and thus a γ is much larger than 1. Due to this relativistic nature, it is reasonable for us to approximate the time (T) required for cosmic-ray muons to travel a distance between two detectors (D) to be:

$$T = Dc^{-1}, \tag{12}$$

regardless of the characteristics of the matter they traverse.

This is one of the key concepts of the muometric positioning system (muPS), a technique similar to GPS in principle. The muPS technique requires, instead of satellites, three or more reference detectors to form the reference coordinate (Fig. 6A). The receiver detector defines the relative position within this coordinate system by using the following relationship:

$$L_i^2 = (x_i - x_p)^2 + (y_i - y_p)^2 + (z_i - z_p)^2, \tag{13}$$

where L_i is the geometrical distance between the ith reference detector located at (x_i, y_i, z_i) and the receiver detector located at (x_p, y_p, z_p). There are two types of device configurations for muometric positioning and navigation: (A) wired positioning and

navigation[4] and (B) wireless positioning and navigation[5,6]. In a wired system, since time synchronization between the reference detector and the receiver detector is a trivial problem, Eq. (13) has only three variables[4]. However, in the wireless system, this time synchronization needs to be done with local clocks that have intrinsic frequency-drift, causing a time offset error (Δt) between the reference clocks and receiver clocks. Therefore, in the wireless system, Eq. (13) will have one more variable such that:

$$L_i^2 = (x_i - x_p)^2 + (y_i - y_p)^2 + (z_i - z_p)^2 + s^2, \qquad\qquad (14)$$

where s ($=c_0\Delta t$) is the pseudo-length that comes from the time offset at the receiver detector[5].

Time synchronization. There are two types of muometric time synchronization techniques: (A) time synchronization using extended air shower (EAS) particles called cosmic time synchronization (CTS)[7,8], and (B) time synchronization using the muon's TOF called cosmic time calibration (CTC)[9]. CTS takes advantage of the simultaneity characteristics of remote EAS particles, which are generated in the Earth's atmosphere and travel to the ground surface (and sometimes beyond). High-energy interactions of the primary cosmic rays with atmospheric nuclei generate cascades of secondaries (electromagnetic cascade and hadronic cascade) called an EAS. The path length difference and variations in the velocities of the secondaries contribute to the shower disk thickness (the longitudinal spread which limits the time synchronization precision of CTS)[7]. However, the difference in their arrival time is smaller than 100 ns when detected on the ground - allowing long-term wireless synchronization of local clocks located within the EAS shower disk. (Figure 6C). On the other hand, CTC uses the cosmic ray muon's well-known travelling speed and the nodal distance values to calibrate local clocks within a sensor network (Figure 6D)[9]. While CTS can synchronize all clocks located inside the area covered by the shower disk (thousands of square-meters) with a nodal distance of $\geq$50 m[8], CTC can synchronize the clocks located within much smaller areas[9]. This is because in regard to CTC, the parameter D in Eq. (12) cannot be too large; hence, $\Delta\theta$, and $\Delta\phi$ in Eq. (11) cannot be too small in order to measure the muon's TOF within a realistic timeframe. On the other hand, with CTC, higher time synchronization precision (sub-nanosecond in principle) is attainable as long as the nodal distance is well known.
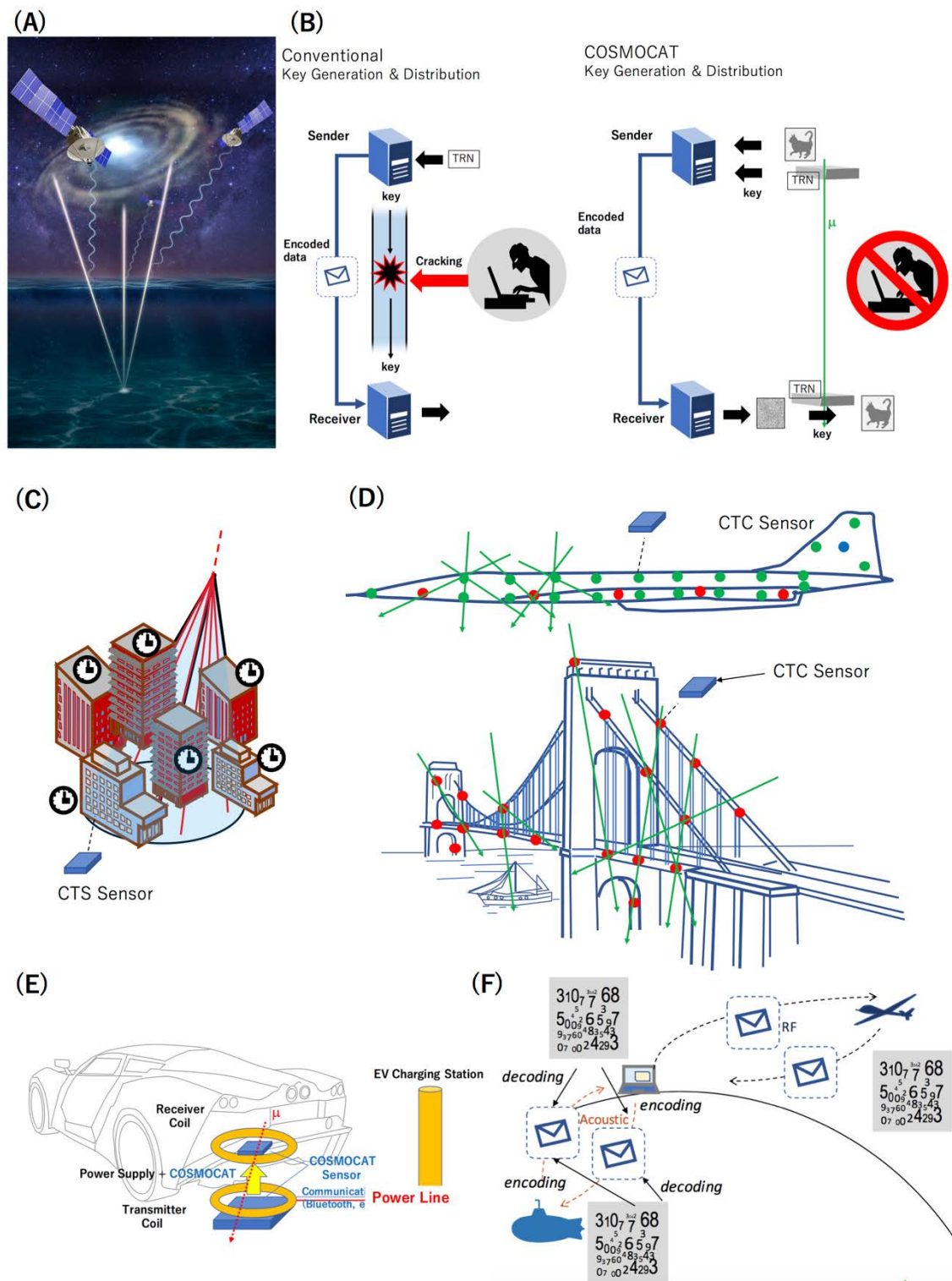
Fig. 6| Muometric PNT and cryptography|. The principle of muPS (A), COSMOCAT (B), CTS (C) and CTC (D) are shown. Applications of CTS, CTC and COSMOCAT are shown by introducing intra-city time synchronization (C), time synchronization of sensor networks in an aircraft (top of D) and a bridge (bottom of D), wireless power transfer (E), and secured UAV/AUV communications (F) as examples. Red dashed and solid lines in (C) indicate a primary particle and EAS particles, respectively. Green arrows in (B) and

(D) and red dotted arrows in (E) indicate cosmic-ray muons.

Cryptography

There have been attempts to generate true random numbers (TRN) using the muon's arrival times or energies deposited to the detector. It is known that cosmic ray muons have a random arrival time distribution: one event occurs completely independently from the occurrence of another event. Ahlen et al.[67] evaluated more than 400,000 high-energy muon arrival times and found no indications of deviations or time anisotropies in the nanosecond to second time scales. However, the intensity of the cosmic muon flux is too small to compete with the generation efficiency of the current state-of-art TRN generators, which can generate 250 trillion TRNs per second. Therefore, it has been thought that cosmogenic TRNs are useless for practical application to our modern communication system. However, on the other hand, no matter how fast we can generate TRNs, if we cannot transfer these TRNs safely, they cannot be used as a basis for a common key cryptosystem.

COSMOCAT is a novel solution for next-generation ultra-high security encryption key generation and distribution (Fig. 6B)[10]. In conventional cryptography, the sender encrypts the data before sending them, and the receiver decrypts the received data. During this process, it is necessary to exchange key information used for encryption and decryption. With COSMOCAT, the sender first creates an encryption key from a random number derived from the time the muon was detected, and subsequently encrypts and transmits the data. High-energy muons travel close to the speed of light, regardless of where they are, and regardless of whether they are indoors or outdoors, on the ground or underground. For this reason, the receiver can estimate the detection time at the sender from the muon's TOF between the sender and the receiver, and consequently, the same encryption key can be generated. Since no physical exchange of the keys occurs, there is no risk of them being stolen on the way; hence the message is uncrackable. If someone tries to duplicate a 24-digit TRN numerical sequence in different locations with the world's best random number-generating machine capable of generating 250 trillion random numbers per second[68] but without data transfer, it would take 3,000 years to accidently generate the same combination of numbers. COSMOCAT can be designed to generate two or more identical 24-digit TRNs in different locations within 0.1 seconds without physically transferring the TRNs.

APPLICATIONS

Muography addresses issues that are broadly relevant to multiple sciences and industries. New tools and ideas continue to emerge from the public or private laboratories devoted to its study. In this section, applications of muographic imaging, muometric PNT, and muogenic cryptography are introduced. Due to space limitations, this review touches upon only a few of the directions where this research may lead.

Muographic imagery

There are several potential applications of muographic imagery (Figure 7A). These include (A) geological investigation of volcanoes[1], landslides[69], mines[70], glaciers[71], etc.,

(B) non-destructive testing, evaluation and monitoring of industrial plants and civil engineering structures such as electric furnace[72], blast furnace[73], nuclear reactors[74,75], railway tunnels[76], underground pillars[77], check valve[78], etc., and (C) non-destructive surveys of cultural heritage, such as pyramids[44,79]. Although it is impossible to introduce all of these applications here, several successful examples will be briefly explained in this section.
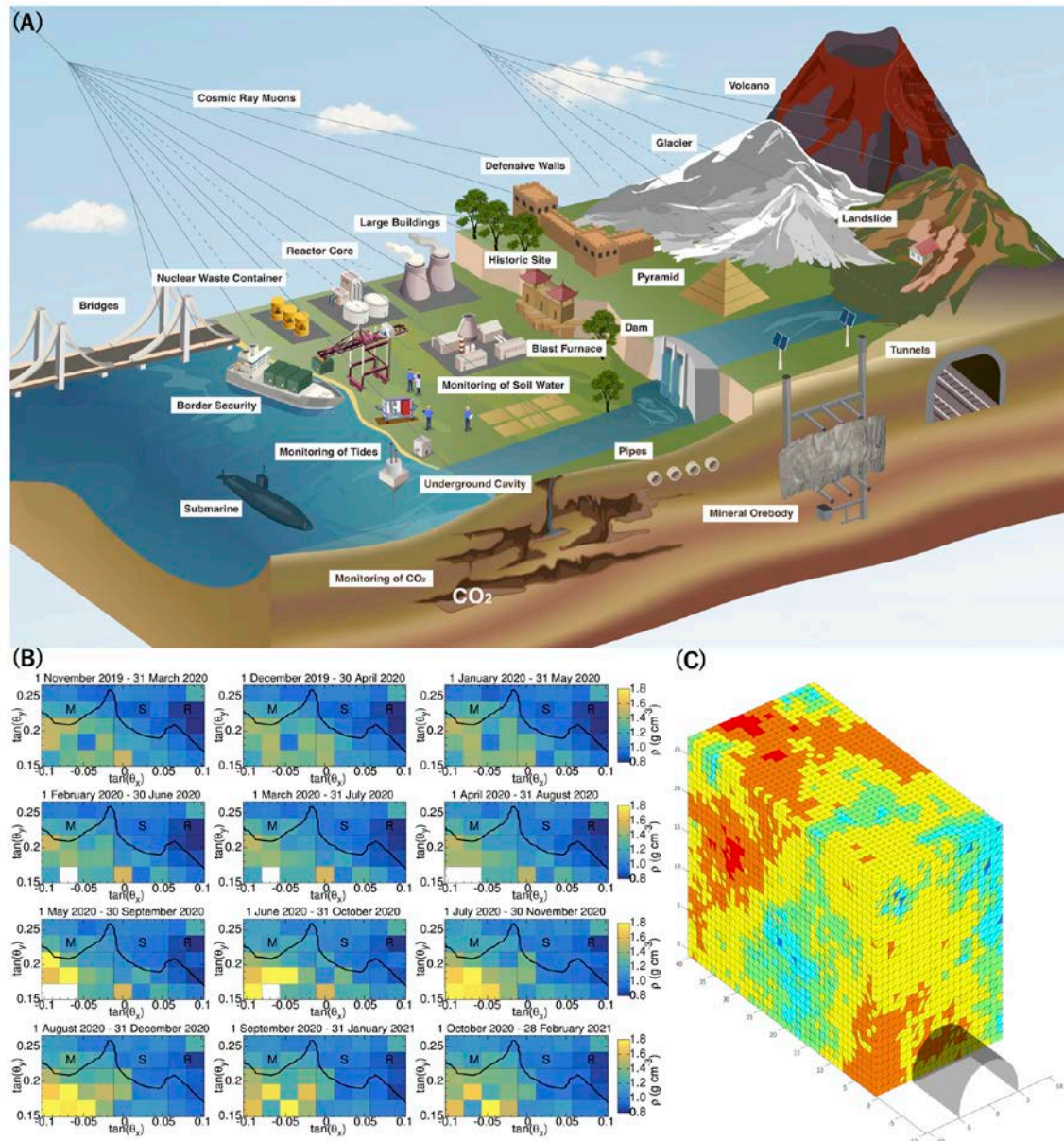
Fig. 7| Applications of muographic imagery| (A) The potential applications of muographic imagery are shown. (B) Time-sequential density images of Sakurajima volcano are shown as an application example of time-sequential imagery. The average density (ρ) values are plotted for the crater region as a function of horizontal and elevation directions for periods of 5 months from November 1, 2018 to February 28, 2021[89]. (C) Online 3D density reconstruction in front of a tunnel-boring machine (TBM) is shown

as an application example of tomography[118]. Each cube is 1m³ volume.

Volcanism. One of the most significant applications of muographic imaging is the visualization of the internal structure of volcanoes. Density is a key property to resolve in order to better understand the more general properties of volcanoes since it is the property that is most readily interpreted in terms of mechanical changes which occur inside volcanoes; hence the reconstruction of density maps can elucidate local-scale geodynamics, such as the movements of magma in the conduit of a volcano. The first important muography experiment in this area focused on the summit of Mount Asama, Japan[80], in 2007. Since then, density distributions have been muographically acquired for several volcanoes including Usu, Japan[81], Showa-Shinzan lava dome, Japan[43], Asama, Japan[80,82,83], Izu peninsula, Japan[84], Omuroyama, Japan[85], Unzen, Japan[86], Shinmoedake, Japan[87], Sakurajima, Japan[88,89], Satsuma-Iwojima, Japan[90,91], La Soufrière, France[92]), Puy de Dome, France[93], Etna, Italy[94], Vesuvius, Italy[30], and Stromboli, Italy[95]. The volcanological targets that can be imaged include magma movements[91], plug formation[89], crater floor collapse[94], hydrothermal deformation[96], and tephra deposition and erosion[97,98]. Recently, muography data have been combined with gravimetry[99,100,101], seismotomography[102]) and satellite-based interferometric synthetic aperture radar (InSAR)[89]. Knowing the magma rise evolution process in the conduit of a volcano as early as possible buys critically important time for initiating alarm and evacuation protocols. Although the technique is limited to horizontal ranges of 2–3 km and is thus applicable only to near-surface depths, muography has been also applied to lava dome formation[81] and collapse[86], magma ascent and decent[91, 103], Vulcanian explosion mechanism[80], magma convection[104], and the tectonic history of peninsula formation[84].

Cultural heritage. Many cultural heritage structures are well suited for muographic imagery. Thus far, muographic surveys have been conducted at cultural heritage structures in Egypt, Italy, China, Indonesia, Japan, and Mexico. Archaeological targets that have been explored range from the Giza pyramids[44], the Imperial mound of Japan[105], the Great Wall of China[106], the Prambanan Temple of Indonesia[107], and the caves of Mt. Echia (ancient settlement ruins) in Naples[108,109].

Some of these works have been dedicated to searching for interior structural anomalies such as large voids[44, 104, 105, 106]. An elongated void inside Khufu's pyramid in Egypt was first reported in 2017 by a muography team[44] and additional data have been collected since then to characterize the void, leading to the recent announcement that its shape is consistent with a corridor-like structure of about 9 m length with a transverse section of about 2 m by 2 m[79]. Confidence in the solidity of these conclusions was given by the addition, since 2020, of measurements with GPR and ultrasonic testing[110]. This motivated finally the visual inspection via an endoscope (borescope), which gave uncontroversial confirmation of the claim. Some experts speculate that it could have been created to redistribute the pyramid's weight around the entrance or another as yet undiscovered chamber[111].

Besides searching for voids, other findings also have brought to light new historical and archaeological implications. For example, a crack formation imaged inside the Imperial mound of Japan indicated the mound deformation caused by translational collapse. These

findings along with the trench survey data indicated that there was an intrinsic problem with the stability of the basic foundation of this mound before the 1596 Fushimi earthquake[105], and it was concluded that changes in the foundation as a response to shaking from the past major earthquake may have produced this large-scale burial mound collapse. Also, the German archaeologist Rolf Klauss[112] compared ancient records of construction and building timescales of the 4th dynasty pyramids with the muographically estimated total weight of the pyramids [113]. This is thought to be an improved approach since measuring cubic units of exposed masonry is not an adequate parameter for accurately determining the correct scale of the pyramid building process. Along with other archaeological evidence, it was concluded that while ancient Egyptian architects could probably build faster and approximate building times for Giza projects, older projects were not finished within similar timeframes[112].

Underground imagery: Groundwater, mining and underground construction. In 2011, groundwater dynamics (as a response to heavy rainfall events) were first captured within a mechanically fractured zone inside a seismic fault[114]. Since then, muographic survey and monitoring activities have been conducted to search for water resources[115], for prevention of landslides (most respond slowly to rainfall and move at low speeds, but have substantial impacts on landscapes after several years)[69], and monitoring of debris flows that are gravity-driven, rapid movements of material composed of a mixture of rock debris and water[97,98]. The main goal of the Tomographic Research of Underground and large STructures with Muographic Expertise (TRUST-ME) project, carried out by the Low Background Noise Underground Research Laboratory of Rustrel (LSBB), is to characterize the dynamics of the water transfer processes in the critical zone, and the cycles of these processes within the region of the Fontaine-de-Vaucluse in particular. It also aims to monitor large water storage infrastructures to enhance safety and operational efficiency. Both objectives address a critical and important societal challenge: sustainable water management[115].

Another application of underground muographic imagery is in mining related investigations. Muographic imaging has not only promising potential for detecting ore deposits[70], but also many open-pit and underground applications in tunnelling and mining projects (e.g., Holma et al.[116]). These include applications such as geological mapping, void detection, drilling and tunnel optimization. Muographic imagery may also improve human safety through the detection and monitoring of faults. For such an application, muography could be used for monitoring unseen structures in front of a tunnel-boring machine (see the following paragraph). In addition, the extent of collapses in underground environments could also be determined by deploying a (or several) muon detector(s) in a somewhat deeper tunnel. Many additional applications in rock mechanics and engineering may also be developed in the future[117].

Tunnel-boring projects require a considerable amount of planning, well ahead of actual drilling operations. Despite these precautionary measures, unexpected geological features (local density variations, cavities, unstable superficial ground, instabilities induced by the driller) often impose further challenges which can only be overcome with real-time adaptations, possibly expensive ones, during drilling operations. Detecting such anomalies prior to physically encountering them requires real-time density analysis which

muography can provide via continuous 3D reconstruction of the geology in front of a tunnel-boring machine (TBM). Since 2017, the Lyon team, France and its startup MUODIM (www.muodim.com) developed the concept and the original reconstruction algorithms for application to the drilling of the "Grand Paris Express" subway network, using scintillator-based muon detectors[118]. Because the muon detector is designed to image structures while moving forward, the muon flux crossing a particular geological object measured by the telescope has different directions to analyze with respect to time, which can be combined to generate 3D density estimates (Figure 7C).

Atmospheric and oceanographic sciences. The target of muography has recently extended to atmospheric and oceanographic objects such as tropic cyclones[119] and tsunamis[120]. The Hyper-Kilometric Submarine Deep Detector (HKMSDD) was installed inside the Trans-Tokyo Bay Expressway underwater tunnel in Japan in order to detect offshore tidal variations[121]. Underwater tunnels allow researchers to exploit the larger muon flux from vertical directions (see equation 6); however, installing HKMSDD into underwater tunnels is not the only way to monitor tide levels. It can also be installed inside near-shore urban underground spaces (UUS) and land lying below sea level (such as many regions in the Netherlands) by utilizing slanted muon detectors to form dense tidal monitor networks[122]. In countries with these conditions, spatiotemporally dense tidal measurements are particularly important for accurately forecasting storm surges[123]. The dense tidal measurements enable more accurate forecasts by assimilating a significant number of observation data. Since muography detectors have no direct contact with water in the above measurement scenarios, maintenance costs are more contained. Moreover, as the muography detectors have no mechanically moving components, the possibility of malfunctions is greatly reduced compared to legacy tide gauge stations, and thus it is easier to realize long and stable operating conditions[123].

Near horizontal muons travelling through the troposphere arrive at a muography detector on the ground after passing through hundreds of kilometers of the atmosphere which may include phenomena such as a tropic cyclone and a mesoscale convective system. Thus, it is possible to measure the internal structure of a cyclone and its movement. For instance, in a recently captured muographically imaged density profile of a tropic cyclone, a low-density region corresponding to the warm core was projected[119]. Since the magnitude of the vertical density difference inside the cyclone indicates the magnitude of the buoyancy, the vertical density profile taken in the midst of a storm is useful for estimating the cyclone's strength. In spite of recent advances in storm tracking prediction, storm intensity forecasting with standard techniques has not comparably advanced. Hence, muography can improve the prediction methodology and alarm systems for storms. This is because the storm track is mostly dependent on the large-scale atmospheric setting that is mainly imaged with satellites, whereas the storm intensity is controlled by the internal dynamics of the cyclone.

In the tropics, the main mechanism that sustains the atmospheric systems is the latent heat released through cumulus convection. One of the major issues to be addressed with respect to the tropical cyclones of the North Indian Ocean is to discover which mechanism (the conditional instability of the second kind (CISK) or the wind-induced surface heat exchange (WISHE) or something else) really controls the convective processes. In a

recent article Tomassini[124] investigated the idea of the interaction between moist convection and atmospheric circulation in tropical storm systems. Unlike the middle and high latitudes, convective mechanisms vary in the tropics, and also vary from season to season and from region to region. Hence, it is of essential importance to identify the exact mechanism of each storm. This lack of understanding can be overcome by applying muographic imagery. For example, a suite of muographic detectors stationed on a coastline where the cyclones make a landfall would be in a position to probe the vertical structure of a tropical cyclone (especially in terms of the vertical velocity field) and the cloud distribution in a cyclone; this could help provide the storm intensity data by providing a series of muographic images.

Planetary sciences. In outer space, resource exploration and volcano monitoring have another vital importance, which is to possibly contribute to securing fundamental assets and improving safety for the development of the first extra-terrestrial human (or robotic) settlements. Despite the various environmental challenges existing on the Moon and Mars[125], muography may be applicable on these planetary bodies[126]. To this end, some muography teams are planning a series of experiments, starting from simulations on Earth, to test the application of muography both in lunar and Martian environments. Tanaka[127] estimated the muon flux on Mars and, subsequently, Kedar *et al*[128] pointed out that since the horizontally integrated density of the Martian atmosphere is ~100 gcm^{-2}, horizontal directions yield more high-energy muons than directions close to the zenith, as opposed to the situation on Earth. This is equivalent to the depth of the terrestrial atmosphere where the muon flux reaches the maximum. A series of experiments is planned in the Atacama Desert, Chile, which may offer one of the best analogous sites for physically simulating the logistics on Mars to operate muon detectors embedded in a rover[129].

PNT
Muometric PNT (Positioning, Navigation and Timing) has important potential for many applications on the Earth since it is already known how helpful GPS-based PNT can be for the technological development of many key sectors of the economy and public security. Muometric techniques offer precise PNT in GPS-denied environments.

Positioning and Navigation. Positioning, navigation and monitoring in indoor, underground, and underwater environments have been modeled and tested. One of the major applications of muometric positioning is monitoring the three-dimensional tectonic or magmatic-driven seafloor motion with a muometric positioning system (muPS) buoy; such a monitoring is not possible with conventional techniques. The muPS buoy equips a reference detector and GPS antenna on the floating section, and the receiver detector is at the anchor section. The reference detector is wired to the receiver detector, and the position of the receiver detector is determined by the slewing motion of the floating section of the buoy. As examples to estimate the size of the detectors and the measurement time required to obtain useful muPS data acquired from the seafloor, Tanaka[4] numerically modeled the following three cases: (A) shallow vertical seafloor displacement caused by the Campi Flegrei volcanic activities reported by Chierici et al.[130], (B) deep seafloor vertical deformation caused by magmatic activities at Axial Seamount reported by Chadwick Jr. et al.[131], and (C) plate tectonics driven deep seafloor horizontal motion reported by Gagnon et al.[132]. Their deformation rates and depths are respectively 3 cm/100

days at -100 m (A), 2 m/10 years at -1500 m (B) and 6 cm/year at -2000 m (C). By assuming these experimental configurations, the following measurements conditions were proposed: Case (A) – 1-m^2 detectors attain 2-4 cm accuracy within 100 days; Case (B) – 4-m^2 detectors attain 10 cm accuracy within 100 days; Case (C) – 20-m^2 detectors attain 5 cm accuracy within 1 year.

One of the most significant applications of wireless muometric navigation (MuWNS) is indoor navigation in environments where GPS is unavailable. Indoor navigation has far-reaching application possibilities, including improved automation within homes, hospitals, offices, factories and mines, etc.[133,134,135,136,137,138,139,140,141,142]. In MuWNS, while the clock of the reference detector could be steered by GPS (See Figure 6A), since the persons to be navigated are likely to be in environments where GPS is unavailable (indoor/underground/underwater), the timing of the muon's arrival at the receiver detector is measured with an independent, high precision local clock located at the receiver detector[5]. Tanaka et al.[6] conducted muometric navigation on the basement floor of a building with a volume of 200 x 100 x 30 m^3. Navigation accuracy achieved by their experiment is summarized in Table 1; the main element causing accuracy problems for MuWNS in this experiment came from relatively large temporal fluctuations (up to ~50 ns) of the local clocks used for the receiver detector. For further improvements of this navigation accuracy, a practical implementation of a chip scale atomic clock (CSAC) will be needed.

Table 1. Comparison of between the currently achieved MuWNS positioning accuracy and single point GNSS/GPS positioning in urban areas reported in prior works

Technique	1 SD error (m) (N-S/E-W)	Max (m) (N-S/E-W)
MuWNS		
Horizontal (Tokyo)	2.3-14.07	6.0-24.21
Vertical (Tokyo)	6.6-9.62	8.0-15.0
(Tanaka et al.[6])		
GPS/GNSS		
Horizontal (Tokyo)	16.1-47.9	102.5-290.7
Vertical (Tokyo)	24.8-115.4	167.8-409.7
(Tominaga & Kubo[143])		
Horizontal (Calgary)	9.4	54.8-97.0
Vertical (Calgary)	7.5-15.1	41.1-204.7
(Angrisano et al.[144])		

Many new technologies have been developed or proposed for underground mine positioning and navigation (see Seguel et al.[145]); muPS has the potential to improve open pit activities and management (e.g., machine control, collision avoidance, fleet management, surveying and drilling). This could be arranged by including a series of muPS-reference stations in fixed positions near the targeted open pit and with muPS receivers in the vehicles themselves. For example, as mining projects advance deeper underground, risks for fracturing and deformation of the space within the mine become greater due to increasing rock pressure. One solution to overcome issues relating to

underground mining is to automate production by using autonomous machines and robots which could be remotely navigated by MuWNS or wired muPS.

Time metrology. Time synchronization techniques are essential systems for time metrology and have even been increasingly considered for applications in fundamental science and commercial sectors. In time metrology, for example, they are employed for the computation of International Atomic Time (TAI) and UTC international atomic time scales, as well as for the remote comparison of national realizations of UTC (i.e., UTC(k))[146]. Timing is also crucial in Fundamental Physics experiments, allowing for increased accuracy of event timestamps and inferring the characteristics of the observed phenomena, depending on their coincidence[147]. In the commercial sector, timing is required – among other options - for synchronizing mobile communication systems, digital radio/TV broadcasts, smart-grids and for accurate/precise timestamps of financial transactions, in agreement with international directives[148]. Time synchronization is typically achieved by means of local oscillators (either high-quality quartz or atomic), informatic protocols over the Internet and/or dedicated optical fibers (e.g., NTP/PTP[149,150], White Rabbit[151], etc., as well as employing satellite techniques[152, 153], with different performances, functional characteristics and limits, reference markets and users. Nowadays, it is becoming imperative to have backup/alternate time synchronization techniques, to increase timing robustness and resilience in critical infrastructures. Based on utilizing the EAS particles, CTS would allow for relatively cheap long-term wireless synchronization of local clocks located within the EAS shower disk, without requiring critical timing information traffic between each CTS sensor and, hence, resistant to jamming and spoofing. An on-site CTS evaluation showed good time synchronization performance at the level of 30-35 ns (SD, 1 σ), over nodal distances of 50-60 m. A long-haul time synchronization technique is possible by forming a daisy chain configuration of CTS sensors, with performances degradation proportion to the square root of the number of nodes[8].

Wireless sensor network and structural health monitoring. Time synchronization of the sensor nodes is a critical function for the optimal operation of wireless sensor networks (WSNs). In particular, very precise WSN time synchronization (< 1 us) is required for measuring the TOF of sound[154], distributing a beamforming array[155], integrating a time-series of proximity detections into a velocity estimate[156], etc. For this, local clocks are incorporated into each node, but they tend to drift. Therefore, recurrent corrections are required. Most of these correction schemes involve clients periodically receiving GPS timing signals from a time server. In principle, Cosmic Time Calibrator (CTC) realizes sub-nanosecond-level time synchronization of WSNs in GPS-denied environments. The recent experimental results have demonstrated that a nodal resynchronization frequency and precision of 60 Hz and ±4.3 ns for a nodal distance of ~ 1m[9] was measured.

Another advantage of CTC is that the clocks inside the RF-shielded box can be recalibrated at the same accuracy. CTC can realize resynchronization of sensor nodes located inside environments where optimal functioning of other RF devices or concepts fail (e.g., time synchronization between the interior of a metal-made aircraft cabin and a metal-made airplane wing or that between aboveground sensors and the underground sensors). This feature enhances the flexibility of WSN deployed for structural health

monitoring (SHM) that requires precise inter-nodal clock synchronization[157]. It also enables precise SHM in a wider variety of locations, with fewer technological limitations and without requiring the use of an active RF source for resynchronization. By removing Wi-Fi or other RF active sources from WSN, the network on the whole becomes more robust; this would make it possible to expand SHM applications to deployment on structures such as supersonic aircrafts, bridges and wind turbines by using sensor nodes that could withstand harsh environments and weather conditions such as rain and snow.

Cryptography

Near-field wireless security. Applications of COSMOCAT to near-field communication (NFC) range from wireless power transfer (WPT) to building automation systems (BAS). COSMOCAT offers an unprecedented high-security key sharing scheme that can be applied to BAS and WPT systems (Fig. 6E). As urban "smartization" expands, short-range wireless communications for sensory operations will be increasingly in demand. However, the security level provided by the currently available wireless techniques for NFC, such as Bluetooth, is too weak to be suitable for applications that transfer sensitive information[158]. WPT is associated with security vulnerabilities like energy stealing and power surge generation that can damage energy receivers since the resonant inductive coupling is very sensitive to other energy receivers near the targeted energy receiver[159,160]. As part of BAS, functions such as lighting operation, air conditioning, escalators, surveillance, water circulation, elevators, and water heating are all targets for automation. In principle, every information packet can be encrypted at a speed of 1.5 Mbps for a receive window size of 256 kb, as long as a configuration shown in Figure 8 is applied. Applying COSMOCAT to this scheme, the size of the buried COSMOCAT sensor would be 1 m^2, while the onboard COSMOCAT sensor would be the size of a presently standard Apple iPad (28 cm x 21 cm); the distance between the two sensors would be 50 cm.

Cloud-based authentication system and secured communication. COSMOCAT can generate a data storage system similar to cloud storage but invincible against hacking as well as other theft and interference tactics. There is a limit to the degree of security assurance for cryptographic keys stored in standard cloud storage [161].This holds true because (A) the storage resources are entirely under the control of the cloud provider[162], (B) potential attackers may generate a new re-encryption key from stored re-encryption keys[163], and (C) there is always a possibility that a third person could physically access and steal the storage assets or storage itself. Quantum key distribution (QKD) has been proposed as a guaranteed and secure method to share private keys between the sender and the receiver. However, QKD only specializes in protecting data on communication lines from attacks, and cannot protect data in storage[164]. QKD may offer highly secured key distribution in principle, but in practice, it cannot be practically used for upgrading the security of authentication and data storage. Tanaka[11] proposed a new invincible authentication system that is applicable to electronic money transactions, e-commerce banking apps, issuing cryptocurrency, and secured communication (Figure 6F) with COSMOCAT-based storage (COSMOCATS). COSMOCAT enables an identical pair of encryption keys to be independently determined without physical key exchange in physically inaccessible servers. Since all information travelling through the traffic is encrypted with many digits of TRN, it is impossible to crack the data. Even a large-scale quantum computer, which may become available in the future, could not crack these

encrypted data in a practical timeframe.

REPRODUCIBILITY AND DATA DEPOSITION

Muographic measurements and observations have been conducted in Europe, Asia, the Americas, and Africa by utilizing the same source: cosmic-ray muons. These measurements/observations can be globally conducted and are reproducible regardless of location. Muographic data are usually stored with a wide range of access policies at each group and at different sites worldwide. However, the datasets used and/or analyzed during the muographic studies are available from these global muographer groups on reasonable request.

LIMITATIONS AND OPTIMIZATIONS

While there still may be a long way to go before muographic techniques are fully standardized, in the past decade pioneer work has already demonstrated the potential of muography. Future challenges may arise from many aspects such as hardware equipment, data analysis software, fieldwork etc.

Hardware

Relatively high-cost hardware. Muographic equipment is usually designed and developed by a comprehensively professional team with members from several interdisciplinary fields, such as particle and nuclear physics, radiation detection, electronics, machinery, and numerical analysis. Currently, particle detection-sensitive materials are rare and costly due to low demand from industry. In addition, some muography hardware systems have a large number of electronic channels, each of which has several functions. These can also be expensive if the system is not designed to be highly integrated. So, as long there is no mass-production, the hardware cost is fairly high compared to other contemporary instruments used in studies in other disciplines.

High complexity and being operated by professionals. The hardware used in applied nuclear science and technology is usually specialized and requires various techniques. Therefore, applying such hardware in field conditions requires engineering and technical professionals. Even with dedicated training, the learning curve for a non-professional may be steeper than what is necessary for using conventional tools in other disciplines.

Portability and all-weather suitability design. Regarding muographic imagery, the on-field scenarios are often rugged and isolated from social infrastructure, and some survey sites may not be easily accessible. Accordingly, features like portability, robustness, ease of deployment, and strength (to withstand harsh weather or environmental conditions) are in demand for field-qualified muographic hardware.

Data analysis software or framework

Lack of generalized tool framework. There are several tools or frameworks available in the muography community, such as particle transportation frameworks using Monte Carlo techniques[20,165], the muon surviving rate calculation tool[166], cosmic ray flux generators[18], forward simulation, and the 3D numerical inversion tool[167,168]. However, as muography continues to evolve, developing a more universal system with a standardized

tool kit is becoming increasingly important. In addition, individual attention to each customized case and professional expertise to perform analysis are needed in almost all applications. Muographic analysis usually involves processing and raw data preparation, signal calibration, forward modelling and inversion etc. Well-trained professionals are required to perform such tasks. In many cases, also experts in the problems to be solved are needed (e.g., geologists, engineers, or archaeologists).

Fieldwork
Long survey duration. An outstanding concern about the need for long-duration surveys is an issue frequently brought up by muography users and researchers. In some scenarios, several weeks or even months may be required to obtain sufficient data statistics, which may not be suitable for specific applications. Temporary changes or dynamic movement in the targeted area may also be challenging to capture for the same reason. Since the cosmic ray muon flux is essentially fixed, the detection system should have a large detection area and high detection efficiency to enhance its capability to speed up imaging.

Feasibility studies before surveying. Since not all structures are suitable for muographic imaging, completing a feasibility study is crucial. A feasibility study must be performed prior to an on-field scan to make sure the task can be successfully performed with the requested resolution and within the proper survey time duration parameters.

OUTLOOK
As seen in Eq. (6), the flux available for muography is proportional to the size of the detector we use. However, the current detector cost per unit area is still too expensive for wide-spread and large-scale implementation. Therefore, one of the critical developments to focus on is the drastic reduction of the detector cost. For example, triangular extrusions along with some of the scintillating pellets drastically reduce the costs required for building online detectors[169]. Producing a 2,000 m^2 detector at a reasonable cost is currently underway in the Exploring the Great Pyramid (EGP) project[28]. In this section, possible future instrumentation for each muographic theme is discussed.

Possible future instrumentation for imaging
There is a demand for muography to image high-temperature objects (>500°C) under high-pressure conditions, for example near or within a geothermal reservoir, a magma chamber or Venusian atmosphere. Scintillation detectors are not an option since plastic scintillators melt under such conditions. To construct a more robust MOS model capable of operating under extreme environmentally hazardous situations, stainless steel welded proportional counters (SPC) could be a good option. Since the structure of each SPC is very simple, being essentially a gas-filled metallic tube with a wire anode, the detector is likely to survive the physically demanding exposure to high temperatures, shocks and vibrations. Plus, SPC was designed for further protection against high pressure. Moreover, the SUS-304 type stainless steel contains Ni and Mo for durability against typical acids. Although at high temperatures, the counter operation is influenced by thermal electrons emitted from the cathode material. Isozumi et al.[170] reported that the maximum operating temperature of their proportional counter was ~800°C when a Fe foil was mounted as a cathode.

In the future, machine-learning-assisted muon spectra analyzers[171] may enable inspection of large-sized meteorite samples such as Gibeon by selecting the momentum of the incident muons. Studying pores inside meteorites is important for determining the size of their origin (asteroids).

Possible future instrumentation for PNT

Navigation. The wireless navigation precision depends on how accurately the muon's TOF can be determined wirelessly. For this, improvements in the wireless logical processing system incorporating CSAC are required. For example, currently available Rubidium CSAC (SPARKX SPX 14830) (1.5 us day^{-1})[172] realizes one order magnitude better drift rate in comparison to OCXO (1.5 us over 4hours)[173], leading to a factor of one order of magnitude better accuracy than what is presented in Table 1. Since the size and the weight are respectively 18.3 x 50.8 x 50.8mm and 55g, it is relatively easy to incorporate into a MuWNS. Although the price is relatively high ($2,000USD/chip), cost is anticipated to be reduced as 5G transforms the network landscape.

Timing. CTS could be potentially conceived as a 'self-adjusting' system, offering high-level continuous (perpetual) performance. In practice, it could work as a backup chain for GPS disciplined oscillators, a standalone standard for frequency and time interval measurements, or as a tool for the dissemination of reference atomic time scales to final users on city-scale areas, with improved characteristics in terms of robustness and reliability, complementary to other time synchronization techniques suitable for critical applications, like optical fibers[174], with the possibility to be retrofitted to be compatible with already existing time synchronization techniques and time protocols (e.g. IRIG-B, CTD, NTP and PTP). Regarding a real use of CTS two possible main categories could be envisaged for users: a) users requiring for precise (and accurate) timestamps, with improved characteristics in terms of robustness and reliability, possibly traceable to a reference time scale (e.g. UTC(k) time scale)[175]. At present, this is carried out by using either NTP/PTP or White Rabbit protocols, among the others. b) Users requiring 1PPS and 10 MHz precise (and accurate) reference signals to be used as a reference for their systems. For both cases a) and b), typical users could belong to scientific communities, as well as to the commercial sectors, already indicated in the previous sections.

Regarding a real use of CTC, particular attention should be addressed in the direction to improve the overall performance of WSNs. Major examples of an important developing WSN technology, include wearable sensors and the structural health monitoring (SHM) system, which are designed to monitor small and large structures such as human body for continuous measurement of human physiological signals, aircraft and civil structures (such as bridges, tunnels, buildings, dams, etc.), where inter-nodal time synchronization is a prerequisite.

In conclusion, muography is an entirely new family of techniques that yields useful and unique information to greatly enhance the robustness of our social infrastructure as well as the understanding of topical natural and man-made targets on the Earth. This Primer on muography has provided a broad overview of the techniques developed in the field of muography and their applications explored around the world in the last decade.

REFERENCES

1. Tanaka, H.K.M. Particle Geophysics. Ann. Rev. Earth Planet. Sci. 42, 535-549 (2014).

2. Liddell, H.G. et al. (1996) A Greek–English Lexicon, Oxford: Clarendon Press

3. Cambridge Dictionary (2023). Retrieved from
https://dictionary.cambridge.org/dictionary/english/radiography

4. Tanaka, H.K.M. Muometric positioning system (µPS) with cosmic muons as a new underwater and underground positioning technique. Sci Rep 10, 18896 (2020). https://doi.org/10.1038/s41598-020-75843-7

5. Tanaka, H.K.M. Wireless muometric navigation system. Sci Rep 12, 10114 (2022). https://doi.org/10.1038/s41598-022-13280-4

6. Tanaka, H.K.M.et al. First Navigation With Wireless Muometric Navigation System (MuWNS) in Indoor and Underground Environments *iScience* (2023) in press.

7. Tanaka, H.K.M. Cosmic time synchronizer (CTS) for wireless and precise time synchronization using extended air showers. Sci Rep 12, 7078 (2022). https://doi.org/10.1038/s41598-022-11104-z

8. Tanaka, H.K.M., Cerretto, G., Gnesi, I. Cosmic Time Synchronization (CTS): first experimental results for a wireless, precise, and perpetual time synchronization system with Extended Air Shower particles. *iScience* 26, 106595 (2023).

9. Tanaka, H.K.M. Cosmic time calibrator for wireless sensor network. Sci Rep 13, 5951 (2023). https://doi.org/10.1038/s41598-023-32262-8

10. Tanaka, H.K.M. Cosmic coding and transfer for ultra high security near-field communications. iS*cience* **26**, 105897 (2023))
https://doi.org/10.1016/j.isci.2022.105897

11. Particle Data Group, Review of Particle Physics. Prog. Theor. Exp. Phys. 2022, 083C01 (2022).

12. Ahlen, S.P. *et al*. Arrival time distributions of very high energy cosmic ray muons in MACRO. *Nucl. Phys. B* **370**, 432-444 (1992).

13. Oláh, L.; Tanaka, H.K.M.; Varga, D. Muography: Exploring Earth's Subsurface with Elementary Particles, Geophysical Monograph 270; American Geophysical Union, John Wiley & Sons, Inc.: Hoboken, NJ, USA, ISBN 9781119723028. (2022)

14. Giammanco, A., et al. Muon Imaging Present Status and Emerging Applications IAEA-TEC-DOC-2012   9789201427229   (2022)

15. Scampoli, P. & Ariga, A. Cosmic Ray Muography, World Scientific, ISBN 9789811264900 (2023)

16. Groom, D. E. *et al*. Muon stopping-power and range tables: 10 MeV–100 TeV. *At. Data Nucl. Data Tables* **78**, 183–356 (2001) https://doi.org/10.1006/adnd.2001.0861

17. D. Heck, *et al.* CORSIKA: a Monte Carlo code to simulate extensive air showers Technical Report FZKA 6019, Forschungszentrum Karlsruhe (1998) https://publikationen.bibliothek.kit.edu/270043064/3813660

18. Hagmann C, et al. Cosmic-ray shower generator (CRY) for Monte Carlo transport codes; proceedings of the 2007 IEEE Nuclear Science Symposium Conference Record, F, (2007).

19. Cillis, A. N. & Sciutto, S. J. Extended air showers and muon interactions. Phys. Rev. D *64*, 013010 (2001) https://doi.org/10.1103/PhysRevD.64.013010

20. Agostinelli, S. *et al.* GEANT4 — a simulation toolkit Nucl. Inst. Methods A, 506, 250-303, (2003) https://doi.org/10.1016/S0168-9002(03)01368-8

21. Antonioli, P. *et al.* A three-dimensional code for muon propagation through the rock: MUSIC Astropart. Phys., 7 (4) (1997), 357, 10.1016/S0927-6505(97)00035-2

22. Niess, V. *et al.* Backward Monte-Carlo applied to muon transport Comput. Phys. Comm., 229 (2018), 54, 10.1016/j.cpc.2018.04.001

23. Tanaka, H.K.M., *et al.* Development of the Cosmic-Ray Muon Detection System for Probing Internal-Structure of a Volcano. *Hyperfine Interactions* **138**, 521–526 (2001). https://doi.org/10.1023/A:1020843100008

24. Tanaka, K.K.M, Nagamine, K., Nakamura, S. N. & Ishida, K. Radiographic measurements of the internal structure of Mt. West Iwate with near-horizontal cosmic-ray muons and future developments. *Nucl. Instr. Meth. Phys. Res. A*, 555, 164-172 (2005). https://doi.org/10.1016/j.nima.2005.08.099

25. Taira, H., Tanaka, H.K.M. A potential space- and power-effective muon sensor module for imaging a volcano. *Earth Planet Space* **62**, 179-186 (2010). https://doi.org/10.5047/eps.2009.06.005

26. Anastasio, A. et al. The MU-RAY detector for muon radiography of volcanoes. *Nucl. Instr. Meth. Phys. Res. A*, 732, 423-426 (2013). https://doi.org/10.1016/j.nima.2013.05.159

27. Lo Presti, D. et al. Development of a scintillation-fiber detector for real-time particle tracking, Journal of Instrumentation, 8, P04015 (2013).

28. Bross A. Tomographic Muon Imaging of the Great Pyramid of Giza, *J. Adv. Instr. Sci.*, 2022, (2022).

29. Marteau, J. et al., Muon tomography applied to geosciences and volcanology, *Nucl. Instr. Meth. Phys. Res. A*, 695 23-28 (2012). https://doi.org/10.1016/j.nima.2011.11.061

30. D'Errico, M. et al. The MURAVES Experiment: A Study of the Vesuvius Great Cone with Muon Radiography, *J. Adv. Instr. Sci.* 2022, 273, (2022). https://doi.org/10.31526/JAIS.2022.273

31. Charpak, G., Bouclier, R., Bressani, T., Favier, J., & Zupancic, C. The use of multiwire proportional counters to select and localize charged particles. *Nucl. Instr. Meth. Phys. Res. A*, 62, 262–268. (1968) https://doi.org/10.1016/0029-554X(68)90371-6

32. Blum,W. and Rolandi,L. Particle Detection with Drift Chambers. Springer-Verlag. (1993)

33. Varga, D., Nyitrai, G., Hamar, G., & Oláh, L. (2016). High efficiency gaseous tracking detector for cosmic muon radiography. Advances in High Energy Physics, 1962317. (2016) https://doi.org/10.1155/2016/1962317

34. Bouteille, S.; Attié, D.; Baron, P.; Calvet, D.; Magnier, P.; Mandjavidze, I.; Winkler, M. A micromegas-based telescope for muon tomography: The WatTo experiment. *Nucl. Instr. Meth. Phys. Res. A*, 834, 223-228. (2016) https://doi.org/10.1016/j.nima.2016.08.002

35. Le Menedeu, E. RPC application in muography and specific developments, JINST, 11, C06009 (2016) https://doi.org/10.1088/1748-0221/11/06/C06009

36. Oláh, L., Tanaka, H. K. M., Ohminato, T., & Varga, D. High-definition and low-noise muography of the Sakurajima volcano with gaseous tracking detectors. Sci. Rep., 8, 3207. (2018) https://doi.org/10.1038/s41598-018-21423-9

37. Nyitrai, G.; Hamar, G.; Varga, D. Toward low gas consumption of muographic tracking detectors in field applications. J. Appl. Phys. 129, 244901 (2021) https://doi.org/10.1063/5.0053984

38. Gera, Á., Nyitrai, G., Surányi, G., Hamar, G. & Varga, D. Gaseous Detectors for Field Applications: Quality Control, Thermal and Mechanical Stability. Instruments 6, 74 (2022) https://doi.org/10.3390/instruments6040074

39. Lázaro Roche, I. A Compact Muon Tracker for Dynamic Tomography of Density Based on a Thin Time Projection Chamber with Micromegas Readout. *Particles* **2021**, *4*, 333-342. DOI:10.3390/particles4030028

40. Aharonian, F. A., Hofmann, W., Konopelko, A. K. & Völk, H.J. The potential of ground based arrays of imaging atmospheric Cherenkov telescopes. I. Determination of shower parameters. Astroparticle Physics 6, 343-368 (1997) https://doi.org/10.1016/S0927-6505(96)00069-2

41. Compagnino, A.A., et al. Evaluating the night sky background directly from the signal images detected by the ASTRI telescopes, Experimental Astronomy, 53, 1017-1035 (2022).

42. Barkas, W.H. *Nuclear research emulsion*, Academic Press, New York, 1973.

43. Tanaka, H.K.M. et al., *Imaging the conduit size of the dome with cosmic-ray muons: The structure beneath Showa-Shinzan Lava Dome, Japan*, Geophys. Res. Lett. **34**, L22311, doi:10.1029/2007GL031389, 2007

44. Morishima K. et al. *Discovery of a big void in Khufu's Pyramid by observation of cosmic-ray muons*. Nature **552**, 386–390 (2017). https://doi.org/10.1038/nature24647, 2017

45. Niwa K. et al., Auto scanning and measuring system for the emulsion chamber, Proc. Int. Cosmic Ray Symp. on High Energy Phenomena, Cosmic Ray Lab. Univ. Tokyo (1974) 149, 1974

46. Aoki S. et al., Fully automated emulsion analysis system, *Nucl. Instrum. Meth. B* 51 , 466 (1990) https://doi.org/10.1016/0168-583X(90)90569-G

47. Nakano, T. Automatic analysis of nuclear emulsion, Ph.D. Thesis, Nagoya University, Japan (1997)

48. Armenise N. et al., High-speed particle tracking in nuclear emulsion by last-generation automatic microscopes, Nuclear Instruments and Methods in Physics Research A 551 (2005) 261–270, https://doi.org/10.1016/j.nima.2005.06.072

49. Arrabito L. et al., Hardware performance of a scanning system for high speed analysis of nuclear emulsions, Nuclear Instruments and Methods in Physics Research A 568 (2006) **2**, 578-587 https://doi.org/10.1016/j.nima.2006.06.072.

50. Bozza C. Final version of SySal2000. (final). Zenodo. Retrieved from https://doi.org/10.5281/zenodo.4271673

51. Bozza C. et al., An integrated system for large scale scanning of nuclear emulsions, Nuclear Instruments and Methods in Physics Research A 703 (2013), 204-212, https://doi.org/10.1016/j.nima.2012.11.099.

52. Morishima K. & Nakano T. Development of a new automatic nuclear emulsion scanning system, S-UTS, with continuous 3D tomographic image read-out, *JINST* 5 P04011, (2010). https://doi.org/10.1088/1748-0221/5/04/P04011

53. Bozza C. et al., GPU-based quasi-real-time Track Recognition in Imaging Devices: from raw Data to Particle Tracks (2014). Retrieved from https://doi.org/10.3204/DESY-PROC-2014-05/2

54. Alexandrov, A. A new generation scanning system for the high-speed analysis of nuclear emulsions, *JINST* 11, P06002 (2016) https://dx.doi.org/10.1088/1748-0221/11/06/P06002

55. Yoshimoto M. et al., Hyper-track selector nuclear emulsion readout system aimed at scanning an area of one thousand square meters, *Progress of Theoretical and Experimental Physics 10*, 103H01 *(*2017) https://doi.org/10.1093/ptep/ptx131

56. Tanaka, H.K.M., et al. Development of a two-fold segmented detection system for near horizontally cosmic-ray muons to probe the internal structure of a volcano Nuclear Instruments and Methods in Physics Research A, 507, 657-669 (2003). https://doi.org/10.1016/S0168-9002(03)01372-X

57. Baccani, G. *et al.* The MIMA project. design, construction and performances of a compact hodoscope for muon radiography applications in the context of archaeology and geophysical prospections JINST, 13 (11) P11001 (2018), 10.1088/1748-0221/13/11/P11001

58. Lázaro Roche, I. *et al.* MUon Survey Tomography based on Micromegas detectors for Unreachable Sites Technology (MUST2): overview and outlook. J. Phys.: Conf. Ser. 1498, 012048 (2020). https://doi.org/10.1088/1742-6596/1498/1/012048

59. Chaiwongkhot, K. *et al.* Development of a portable muography detector for infrastructure degradation investigation, IEEE Trans. Nucl. Sci., 65, 2316 (2018). 10.1109/TNS.2018.2855737

60. Hamar, G. et al, Underground muography with portable gaseous detectors, in Journal of Physics: Conference Series, 2374, 012186 (2022) https://doi.org/10.1088/1742-6596/2374/1/012186

61. Gamage, R.M.I.D. et al. A portable muon telescope for multidisciplinary applications. JINST, 17, C01051 (2022) https://doi.org/10.1088/1748-0221/17/01/C01051

62. Yifan, Z. et al. Discrimination of drugs and explosives in cargo inspections by applying machine learning in muon tomography, High Power Laser Part. Beams 30 086002 (2018).

63. Mahon, D., et al., First-of-a-kind muography for nuclear waste characterization, Philos. Trans. R. Soc. London, Ser. A 377 2137 20180048 (2019).

64. Barnes, S. et al. Cosmic-Ray Tomography for Border Security, Instruments 7, 13 (2023).

65. Bikit, I. et al. Novel approach to imaging by cosmic-ray muons. *EPL* **113** 58001 (2016) https://iopscience.iop.org/article/10.1209/0295-5075/113/58001

66. Department of Homeland Security. Positioning, Navigation, and Timing (PNT) Program (2023). Retrieved from https://www.dhs.gov/science-and-technology/pnt-program.

67 Ahlen S.P. et al. Arrival time distributions of very high energy cosmic ray muons in MACRO Nucl. Phys. B, 370, 432-444 (1992).

68 Kim, K. *et al*. Massively parallel ultrafast random bit generation with a chip-scale laser. *Science* **371**, 948–952 (2021).

69. Tanaka, H. K. M. and Sannomiya, A.: Development and operation of a muon detection system under extremely high humidity environment for monitoring underground water table, Geosci. Instrum. Method. Data Syst., 2, 29-34 (2013). https://doi.org/10.5194/gi-2-29-2013

70. Schouten, D. & Ledru, P. Muon Tomography Applied to a Dense Uranium Deposit at the McArthur River Mine. *J. Geophys. Res. Solid Earth* **123,** 8637–8652 (2018). https://doi.org/10.1029/2018JB015626

71. Nishiyama R. et al., *First measurement of ice-bedrock interface of alpine glaciers by cosmic muon radiography*, Geophys. Res. Lett., 44,6244–6251, https://doi.org/10.1002/2017GL073599

72. Tanaka, H. K. M. Development of stroboscopic muography. Geosci. Instrum. Method. Data Syst., 2, 41–45, 2013www.geosci-instrum-method-data-syst.net/2/41/2013/doi:10.5194/gi-2-41-2013

73. Nagamine, K. et al. Probing the inner structure of blast furnaces by cosmic-ray muon radiography. Proceedings of the Japan Academy, Series B, 81, 275-260 (2005) https://doi.org/10.2183/pjab.81.257

74. Procureur, S. et al. 3D imaging of a nuclear reactor using muography measurements. Science Advances, 9, eabq8431 (2023). https://doi.org/10.1126/sciadv.abq8431

75. Morishima, K. *Visualization of molten debris of Fukushima Daiichi Nuclear Power Plant by cosmic ray muon radiography*. Oyo Butsuri, 86(11), 950-955, (2017).

76. Thompson, L. F., et al. Muon tomography for railway tunnel imaging. Phys. Rev. Research 2, 023017 (2020). https://doi.org/10.1103/PhysRevResearch.2.023017

77. Oláh, L. et al. The first prototype of an MWPC-based borehole-detector and its application for muography of an underground pillar. Butsuri-Tansa, 71, 161-168 (2018) https://doi.org/10.3124/segj.71.161

78. Durham, J. M. et al. Tests of cosmic ray radiography for power industry applications. AIP Advances, 5, 067111-1-8 (2015) http://doi.org/10.1063/1.4922006

79. Procureur, S., Morishima, K., *et al.* Precise characterization of a corridor-shaped structure in Khufu's Pyramid by observation of cosmic-ray muons. *Nat Commun* **14**, 1144 (2023). https://doi.org/10.1038/s41467-023-36351-0

80. Tanaka, H. K. M. *et al.* High resolution imaging in the inhomogeneous crust with cosmic-ray muon radiography: The density structure below the volcanic crater floor of Mt. Asama. *Japan. Earth Planet. Sci. Lett.* **263**, 104–113. (2007). https://doi.org/10.1016/j.epsl.2007.09.001

81. Kusagaya, T. & Tanaka, H. K. M. Muographic imaging with a multi-layered telescope and its application to the study of the subsurface structure of a volcano. *Proc. Jpn. Acad. Ser. B* **91**, 501–510. (2015). https://doi.org/10.2183/pjab.91.501

82. Tanaka, H. K. M., Uchida, T., Tanaka, M., Shinohara, H., & Taira, H. Cosmic-ray muon imaging of magma in conduit: Degassing process of Satsuma-Iwojima Volcano, Japan. *Geophysical Research Letters*, 36, L01304 (2009). https://doi.org/10.1029/2008GL036451

83. Tanaka, H.K.M. et al. Three-dimensional computational axial tomography scan of a volcano with cosmic ray muon radiography. JOURNAL OF GEOPHYSICAL RESEARCH, 115, B12332 (2010) https://doi.org/10.1029/2010JB007677

84. Tanaka, H. Muographic mapping of the subsurface density structures in Miura, Boso and Izu peninsulas, Japan. *Sci Rep* **5**, 8305 (2015). https://doi.org/10.1038/srep08305

85. Miyamoto, S. et al., *A muographic study of a scoria cone from 11 directions using nuclear emulsion cloud chambers*, Geosci. Instrum. Method. Data Syst., 11, 127-147, (2022). https://doi.org/10.5194/gi-11-127-2022

86. Tanaka, H. Instant snapshot of the internal structure of Unzen lava dome, Japan with airborne muography. *Sci Rep* **6**, 39741 (2016). https://doi.org/10.1038/srep39741

87. Kusagaya, T. & Tanaka, H.K.M. Development of the very long-range cosmic-ray muon radiographic imaging technique to explore the internal structure of an erupting volcano, Shinmoe-dake, Japan. Geosci. Instrum. Method. Data Syst., 4, 215-226 (2015). www.geosci-instrum-method-data-syst.net/4/215/2015/

88. Oláh, L., & Tanaka, H.K.M. Machine Learning with Muographic Images as Input: an Application to Volcano Eruption Forecasting. Geophysical Monogaph 270, 43-54, (2022) https://doi.org/10.1002/9781119722748.ch4

89. Oláh, L., et al. Muon imaging of volcanic conduit explains link between eruption frequency and ground deformation. Geophysical Research Letters, 50, e2022GL101170 (2023). https://doi.org/10.1029/2022GL101170

90. Tanaka, H.K.M., et al. Cosmic-ray muon imaging of magma in a conduit: Degassing processof Satsuma-Iwojima Volcano, Japan. Geophysical Research Letters, 36, L01304 (2009). https://doi.org/10.1029/2008GL036451

91. Tanaka, H., Kusagaya, T. & Shinohara, H. Radiographic visualization of magma dynamics in an erupting volcano. *Nat Commun* **5**, 3381 (2014). https://doi.org/10.1038/ncomms4381

92. Lesparre, N. et al. Density muon radiography of La Soufrière of Guadeloupe volcano: comparison with geological, electrical resistivity and gravity data. Geophysical Journal International, 190, 1008-1019 (2012). https://doi.org/10.1111/j.1365-246X.2012.05546.x

93. Ambrosino, F., et al. Joint measurement of the atmospheric muon flux through the Puy de Dôme volcano with plastic scintillators and resistive plate chambers detectors. Journal of Geophysical Research: Solid Earth, 120, 7290-7307 (2015). https://doi.org/10.1002/2015JB011969

94. Lo Presti, D., *et al.* Muographic monitoring of the volcano-tectonic evolution of Mount Etna. *Sci Rep* **10**, 11351 (2020). https://doi.org/10.1038/s41598-020-68435-y

95. Tioukov, V., *et al.* First muography of Stromboli volcano. *Sci Rep* **9**, 6695 (2019). https://doi.org/10.1038/s41598-019-43131-8

96. Jourde, K., *et al.* Muon dynamic radiography of density changes induced by hydrothermal activity at the La Soufrière of Guadeloupe volcano. *Sci Rep* **6**, 33406 (2016). https://doi.org/10.1038/srep33406

97. Tanaka, H.K.M. Development of the muographic tephra deposit monitoring system. *Sci Rep* **10**, 14820 (2020). https://doi.org/10.1038/s41598-020-71902-1

98. Oláh, L., Tanaka, H.K.M. & Hamar, G. Muographic monitoring of hydrogeomorphic changes induced by post-eruptive lahars and erosion of Sakurajima volcano. *Sci Rep* **11**, 17729 (2021). https://doi.org/10.1038/s41598-021-96947-8

99. Okubo, S. & Tanaka, H.K.M. Imaging the density profile of a volcano interior with cosmic-ray muon radiography combined with classical gravimetry. Meas. Sci. Technol. 23, 042001 (2012). https://doi.org/10.1088/0957-0233/23/4/042001

100. Nishiyama, R. *et al.* Integrated processing of muon radiography and gravity anomaly data toward the realization of high-resolution 3-D density structural analysis of volcanoes: Case study of Showa-Shinzan lava dome. *Usu. Japan. JGR Solid Earth* **119**, 699-710 (2014). https://doi.org/10.1002/2013JB010234

101. Rosas-Carbajal, M. *et al*. Three-dimensional density structure of La Soufrière de Guadeloupe lava dome from simultaneous muon radiographies and gravity data. *Geophysical Research Letters* **44**, 6743–6751 (2017). https://doi.org/10.1002/2017GL074285

102. Le Gonidec, Y., *et al.* Abrupt changes of hydrothermal activity in a lava dome detected by combined seismic and muon monitoring. *Sci Rep* **9**, 3079 (2019). https://doi.org/10.1038/s41598-019-39606-3

103. Leone, G., et al. Muography as a new complementary tool in monitoring volcanic hazard: implications for early warning systems. Proc. R. Soc. A 477:20210320 (2021) https://doi.org/10.1098/rspa.2021.0320

104. Shinohara, H. & Tanaka, H.K.M. Conduit magma convection of a rhyolitic magma: Constraints from cosmic-ray muon radiography of Iwodake, Satsuma-Iwojima volcano, Japan. Earth and Planetary Science Letters, 349-350, 87–97 (2012). http://dx.doi.org/10.1016/j.epsl.2012.07.002

105. Tanaka, H. K. M., Sumiya, K., and Oláh, L.: Muography as a new tool to study the historic earthquakes recorded in ancient burial mounds, Geosci. Instrum. Method. Data Syst., 9, 357-364, (2020). https://doi.org/10.5194/gi-9-357-2020

106. Liu, G. et al. High-precision muography in archaeogeophysics: A case study on Xi'an defensive walls. Journal of Applied Physics 133, 014901 (2023) https://doi.org/10.1063/5.0123337

107. Hanazato, T. et al. Muon radiography Monitoring for Structural Survey of the Prambanan World Heritage Temple. Japan Geoscience Union, Kanagawa, (2014).

108. Saracino, G., Amato, L., Ambrosino, F. *et al.* Imaging of underground cavities with cosmic-ray muons from observations at Mt. Echia (Naples). *Sci Rep* **7**, 1181 (2017). https://doi.org/10.1038/s41598-017-01277-3

109. Cimmino, L., Baccani, G., Noli, P. *et al.* 3D Muography for the Search of Hidden Cavities. *Sci Rep* **9**, 2974 (2019). https://doi.org/10.1038/s41598-019-39682-5

110. M. Elkarmoty et al., "Localization and shape determination of a hidden corridor in the Great Pyramid of Giza using non-destructive testing", NDT & E International 102809 (2023).

111. BBC Egypt: Hidden corridor in Great Pyramid of Giza seen for first time (2023) Retrieved from https://www.bbc.com/news/world-middle-east-64825526.

112. Klauss, R. Lifting Work and Building Time at the 4th Dynasty Pyramids. Trabajos de Egiptología 12, 85-111 (2021).

113. Tanaka, H.K.M. & Ohshiro, M. Muographic data analysis method for medium-sized rock overburden inspections. Geosci. Instrum. Method. Data Syst., 5, 427-435 (2016). https://doi.org/10.5194/gi-5-427-2016

114. Tanaka, H.K.M., et al. Cosmic muon imaging of hidden seismic fault zones: Rainwater permeation into the mechanical fractured zones in Itoigawa–Shizuoka Tectonic Line, Japan. Earth and Planetary Science Letters, 306, 156-162 (2011). https://doi.org/10.1016/j.epsl.2011.03.036

115. Lázaro Roche, I., et al. Water Resource Management: The Multi-Technique Approach of the Low Background Noise Underground Research Laboratory and its Muon Detection Projects. Geophysical Monograph 270, 137-152 (2022). https://doi.org/10.1002/9781119722748.ch10

116. Holma, M., Zhang, Z.-X., Kuusiniemi, P., Loo, K. & Enqvist, T. Future Prospects of Muography for Geological Research and Geotechnical and Mining Engineering. Geophysical Monograph 270, 199-219 (2022).

https://doi.org/10.1002/9781119722748.ch15

117. Zhang, Z.-X., Enqvist, T., Holma, M. & Kuusiniemi, P. Muography and its potential applications to mining and rock engineering. Rock Mechanics and Rock Engineering 53, 4893-4907 (2022). https://doi.org/10.1007/s00603-020-02199-9

118. Marteau, J., et al. Development of Scintillator-Based Muon Detectors for Muography. Geophysical Monograph 270, 237-252 (2022). https://doi.org/10.1002/9781119722748.ch17

119. Tanaka, H.K.M., et al. Atmospheric muography for imaging and monitoring tropic cyclones. Sci Rep 12, 16710 (2022). https://doi.org/10.1038/s41598-022-20039-4

120. Tanaka, H.K.M., Aichi, M., Balogh, S.J. et al. Periodic sea-level oscillation in Tokyo Bay detected with the Tokyo-Bay seafloor hyper-kilometric submarine deep detector (TS-HKMSDD). Sci Rep 12, 6097 (2022). https://doi.org/10.1038/s41598-022-10078-2

121. Tanaka, H. K. et al. First results of undersea muography with the Tokyo-Bay seafloor hyper-kilometric submarine deep detector. Sci. Rep. 11, 19485 (2021). https://doi.org/10.1038/s41598-021-98559-8

122. Tanaka, H.K.M. Muography for a dense tide monitoring network. Sci Rep 12, 6725 (2022). https://doi.org/10.1038/s41598-022-10373-y

123. Verlaan, M. et al. Operational storm surge forecasting in the Netherlands: Developments in the last decade. Philos. Trans. R. Soc. A 363, 1441-1453 (2005). https://doi.org/10.1098/rsta.2005.1578

124. Tomassini, L. The Interaction between Moist Convection and the Atmospheric Circulation in the Tropics. Bulletin of the American Meteorological Society. 101, E1378–E1396 (2022). https://doi.org/10.1175/BAMS-D-19-0180.1

125. Leone, G., Ahrens, C., Calabrese, G., Tanaka, H. K. M. & D'Incecco, P. in *Mars: A Volcanic World* 309–323 (Springer International Publishing, 2021). doi:10.1007/978-3-030-84103-4_12

126. Holma, M., Joutsenvaara, J. & Kuusiniemi, P. Astroparticle physics obtaining more attention from a new type of audience. *J. Phys. Conf. Ser.* **2156,** 12178 (2021).

127. Tanaka, H.K.M. Monte-Carlo simulations of atmospheric muon production: Implication of the past martian environment. Icarus, 191, 603-615 (2007). https://doi.org/10.1016/j.icarus.2007.05.014

128. Kedar, S. *et al.* Muon radiography for exploration of Mars geology. *Geosci. Instrumentation, Methods Data Syst.* **2,** 157–164 (2013).

129. Azua-Bustos, A., González-Silva, C. & Fairén, A. G. The Atacama Desert in

Northern Chile as an Analog Model of Mars. *Front. Astron. Sp. Sci.* **8,** 242 (2022).

130. Chierici, F. et al. A new method to assess long-term sea-bottom verticaldisplacement in shallow water using a bottom pressuresensor: application to Campi Flegrei, Southern Italy. J. Geophys. Res. 121, 7775–7789 (2016).

131. Chadwick, W. W., Nooner, S. L., Butterfield, D. A. & Lilley, M. D. Seafloor deformation and forecasts of the April 2011 eruption at Axial Seamount. Nat. Geosc. 5, 474–477 (2012).

132. Gagnon, K., Chadwell, C. D. & Norabuena, E. Measuring the onset of locking in the Peru-Chile trench with GPS and acoustic measurements. Nature 434, 205–208 (2005).

133. Kosaka, A. and Kak, A.C. Fast Vision-Guided Mobile Robot Navigation Using Model-Based Reasoning and Prediction of Uncertainties. Comput. Vis. Image. Underst., *56*, 271-329 (1992).

134. Lu, F. & Milios, E. Robot pose estimation in unknown environments by matching 2D range scans, J. Intell. Robot. Syst., vol. 18, no. 3, pp. 249–275, Mar. 1997.

135. Motomura, A. et al. Real-time self-localization method by using measurements of directions of two landmarks and dead reckoning. J. Robot. Soc. Jpn. *23*, 39–48 (2005).

136. Hakim, S. et al. A mobile system for indoors 3-D mapping and positioning. in Proc. 4th Conf. Optical 3-D Meas. Techn. 275–282 (1997).

137. Sertatil, C. et al. A novel acoustic indoor localization system employing CDMA. Digit. Sig. Process. *22*, 506-517 (2012).

138. Hahnel, D. et al. Learning compact 3d models of indoor and outdoor environments with a mobile robot. in Proc. 4th EUROBOT, 2001, 91–98 (2001).

139. Kelly, A. General solution for linearized systematic error propagation in vehicle odometry. in Proc. IEEE/RSJ IROS, 2001, 1938–1945 (2001).

140. Crowley, J. L. Asynchronous control of orientation and displacement in a robot vehicle. in Proc. IEEE Int. Conf. Robot. Autom. 1277–1282 (1989).

141. Kataria, S. et al. Survey Paper on Wireless Underground Positioning System International Journal of Computer Applications *130*, 1-4 (2015).

142. Chow, J. F. et al. Toward Underground Localization: Lidar Inertial Odometry Enabled Aerial Robot Navigation. arXiv:1910.13085v1 (2019).

143. Tominaga, T. & Kubo, N. Adaptive Estimation of Measurement Noise to Improve the Performance of GNSS Single Point Positioning in Dense Urban Environment, Journal of IPNT, *8*, 1-8 (2017).

144. Angrisano, A. et al. Adaptive Estimation of Measurement Noise to Improve the Performance of GNSS Single Point Positioning in Dense Urban Environment. Acta. Geod. Geophys. *48*,149–161 (2013).

145. Seguel, F. et al. Underground Mine Positioning: A Review. IEEE Sensors Journal 22(6), 4755 - 4771 (2022). doi:10.1109/JSEN.2021.3112547.

146. Panfilo G. & Arias F. The Coordinated Universal Time. Metrologia, 56, 042001 (2019). DOI 10.1088/1681-7575/ab1e68

147. Cerretto, G. et al. Extensive cosmic showers detection: the importance of timing and the role of GPS in the EEE experiment. GPS Solutions 25, 125 (2021). https://doi.org/10.1007/s10291-021-01152-9.

148. Directive 2014/65/EU of the European Parliament and of the Council of 15 May 2014 on markets in financial instruments and amending Directive 2002/92/EC and Directive 2011/61/EU (recast) (Text with EEA relevance) - https://eur-lex.europa.eu/legal-content/EN/ALL/?uri=CELEX%3A32014L0065

149. Smotlacha, V. et al. On calibration of network time services. Metrologia, 45, S51 (2008). DOI 10.1088/0026-1394/45/6/S09

150. Mkacher F. & Duda A. Calibrating NTP. 2019 IEEE International Symposium on Precision Clock Synchronization for Measurement, Control, and Communication (ISPCS), Portland, OR, USA, 2019, pp. 1-6, doi: 10.1109/ISPCS.2019.8886646.

151. The White Rabbit Official CERN website: https:// white-rabbit.web.cern.ch/

152. Petit G. & Jiang Z. GPS All in View time transfer for TAI computation. Metrologia, 45, 35 (2008). DOI 10.1088/0026-1394/45/1/006

153. Jiang, Z. & Petit, G. Combination of TWSTFT and GNSS for accurate UTC time transfer. Metrologia, 46, 305 (2009). DOI 10.1088/0026-1394/46/3/019

154. Merrill, W. *et al*. Autonomous Position Location in Distributed, Embedded, Wireless Systems. Retrieved from http://www.sensoria.com/publications.html.

155. Wang, H. *et al*. A Wireless Time-Synchronized COTS Sensor Platform Part II–Applications to Beamforming. Retrieved from http://lecs.cs.ucla.edu/Publications.

156. Cerpa, A. *et al*. Habitat monitoring: Application driver for wireless communications technology. Retrieved from http://www.isi.edu/scadds/papers/CostaRica-oct01-final.ps.

157. Sazonov, E. *et al*. Wireless intelligent sensor and actuator network—A scalable platform for time synchronous applications of structural health monitoring. *Struct. Health Monitor.* **9**, 465–476 (2010).

158. Gehrmann, C. (2002) Bluetooth Security Bluetooth SIG Security Expert Group, White Paper, Apr. 1, 2002.

159. Zhang, Z. et al. (2011) Improvement of Electromagnetic Compatibility of Motor Drives Using Hybrid Chaotic Pulse Width Modulation. IEEE Trans. Magn. *47*, 4018–4021.

160. Ye, S. & Chau, K.T. (2007) Chaoization of DC Motors for Industrial Mixing. IEEE Trans. Ind. Electron. *54*, 2024–2032.

161. Prajapati, P & Shah, P. A Review on Secure Data Deduplication: Cloud Storage Security Issue. *J. King Saud Univ. - Comput. Inf. Sci.* **34**, 3996-4007 (2022).

162. National Institute of Standards and Technology, Cryptographic Key Management Issues & Challenges in Cloud Services (2013). Retrieved from https://nvlpubs.nist.gov/nistpubs/ir/2013/nist.ir.7956.pdf

163. Lin, H-Y. & Tzeng W-G. A Secure Erasure Code-Based Cloud Storage System with Secure Data Forwarding. *IEEE Trans. Parallel Distrib. Syst.* **23**, 995 - 1003 (2012).

164. National Cyber Security Centre. Quantum security technologies (2016). Retrieved from https://www.ncsc.gov.uk/whitepaper/quantum-security-technologies

165. Battistoni G et al. Overview of the FLUKA code. Annals Nucl Energy 82, 10-8 (2015).

166. Kudryavtsev. V. A. Muon simulation codes MUSIC and MUSUN for underground physics. Computer Physics Communications 180(3) 339-46 (2009).

167. Cockett, R. et al. SimPEG: An open source framework for simulation and gradient based parameter estimation in geophysical applications. Computers & Geosciences, 85, 142-54 (2015).

168. Rücker C, et al. An open-source library for modelling and inversion in geophysics. Computers and Geosciences, 109, 106-23 (2017).

169. Pla-Dalmau, A. et al. Low-cost extruded plastic scintillator, Nucl. Instr. Meth. Phys. Res. A, 466, 482-491 (2001).

170. Isozumi, Y. *et al.* High-temperature proportional counter and its application to resonance–electron Mössbauer spectroscopy. *Sci. Instrum.* **52**, 413 (1981) https://doi.org/10.1063/1.1136595

171. Oláh, L. et al. Development of Machine Learning-Assisted Spectra Analyzer for the NEWCUT Muon Spectrometer. Journal of Advanced Instrumentation in Science, 2022, JAIS-264 (2022). https://doi.org/10.31526/jais.2022.264

172. Sparkfun. Atomic Clock Out of stock SPX-14830 (2023). Retrieved from https://www.sparkfun.com/products/14830

173. Microtron. Trimble Thunderbolt PTP GM200 (2023). Retrieved from https://www.microtron.be/media/c78fa7db61fd72aec4c52d1a2ae40826/thunderbolt-ptp-grandmaster-clock-ptp-gm200.pdf

174. Insero, G. et al. Measuring molecular frequencies in the 1–10 μm range at 11-digits accuracy. Sci Rep 7, 12780 (2017). https:// doi.org/10.1038/s41598-017-12891-6.

175. Bertacco, E.K. et al. Latest improvements at INRIM Time Laboratory". Proceedings of the 51st Annual Precise Time and Time Interval Systems and Applications Meeting. 2020, San Diego, CA (USA). https:// doi.org/10.33012/2020.17296.

Related Links
MUOGRAPHIX: https://news.muographix.u-tokyo.ac.jp/